Machine Vision and Applications (1988) 1:127–152

Machine Vision and Applications

Active, Optical Range Imaging Sensors

Paul J. Besl
Computer Science Department, General Motors Research Laboratories, Warren, Michigan 48090-9055 USA

Abstract: Active, optical range imaging sensors collect three-dimensional coordinate data from object surfaces and can be useful in a wide variety of automation applications, including shape acquisition, bin picking, assembly, inspection, gaging, robot navigation, medical diagnosis, and cartography. They are unique imaging devices in that the image data points explicitly represent scene surface geometry in a sampled form. At least six different optical principles have been used to actively obtain range images: (1) radar, (2) triangulation, (3) moire, (4) holographic interferometry, (5) focusing, and (6) diffraction. In this survey, the relative capabilities of different sensors and sensing methods are evaluated using a figure of merit based on range accuracy, depth of field, and image acquisition time.

Key Words: range image, depth map, optical measurement, laser radar, active triangulation

1. Introduction

Range-imaging sensors collect large amounts of three-dimensional (3-D) coordinate data from visible surfaces in a scene and can be used in a wide variety of automation applications, including object shape acquisition, bin picking, robotic assembly, inspection, gaging, mobile robot navigation, automated cartography, and medical diagnosis (biostereometrics). They are unique imaging devices in that the image data points explicitly represent scene surface geometry as sampled points. The inherent problems of interpreting 3-D structure in other types of imagery are not encountered in range imagery although most low-level problems, such as filtering, segmentation, and edge detection, remain.

Most active optical techniques for obtaining range images are based on one of six principles: (1) radar, (2) triangulation, (3) moire, (4) holographic interferometry, (5) lens focus, and (6) Fresnel diffraction. This paper addresses each fundamental category by discussing example sensors from that class. To make comparisons between different sensors and sensing techniques, a performance figure of merit is defined and computed for each representative sensor if information was available. This measure combines image acquisition speed, depth of field, and range accuracy into a single number. Other application-specific factors, such as sensor cost, field of view, and standoff distance are not compared.

No claims are made regarding the completeness of this survey, and the inclusion of commercial sensors should not be interpreted in any way as an endorsement of a vendor's product. Moreover, if the figure of merit ranks one sensor better than another, this does not necessarily mean that it is better than the other for any given application.

Jarvis (1983b) wrote a survey of range-imaging methods that has served as a classic reference in range imaging for computer vision researchers. An earlier survey was done by Kanade and Asada (1981). Strand (1983) covered range imaging techniques from an optical engineering viewpoint. Several other surveys have appeared since then (Kak 1985, Nitzan et al. 1986, Svetkoff 1986, Wagner 1987). The goal of this survey is different from previous work in that it provides a simple example methodology for quantitative performance comparisons between different sensing methods which may assist system engineers in performing evaluations. In addition, the state of the art in range imaging advanced rapidly in the past few years and is not adequately documented elsewhere.

This survey is structured as follows. Definitions of range images and range-imaging sensors are given first. Different forms of range images and generic viewing constraints and motion requirements are discussed next followed by an introduction to sensor performance parameters, which are then used to define a figure of merit. The main body sequentially addresses each fundamental ranging method. The figure of merit is computed for each sensor if possible. The conclusion consists of a sen-

sor comparison section and a final summary. An introduction to laser eye safety is included in the appendix. This paper is an abridged version of Besl (1988), which was derived from sections of Besl (1987). Tutorial material on range-imaging techniques may be found in both as well as in the references.

2. Preliminaries

A *range-imaging sensor* is any combination of hardware and software capable of producing a *range image* of a real-world scene under appropriate operating conditions. A *range image* is a large collection of *distance measurements* from a known reference coordinate system to *surface points* on object(s) in a *scene*. If scenes are defined as collections of physical objects and if each *object* is defined by its mass density function, then surface points are defined as the 3-D points in the half-density level set of each object's normalized mass-density function as in Koenderink and VanDoorn (1986). Range images are known by many other names depending on context: range map, depth map, depth image, range picture, rangepic, 3-D image, 2.5-D image, digital terrain map (DTM), topographic map, 2.5-D primal sketch, surface profiles, *xyz* point list, contour map, and surface height map.

If the distance measurements in a range image are listed relative to three orthogonal coordinate axes, the range image is in *xyz* form. If the distance measurements indicate range along 3-D direction vectors indexed by two integers (i, j), the range image is in r_{ij} form. Any range image in r_{ij} form can be converted directly to *xyz* form, but the converse is not true. Since no ordering of points is required in the *xyz* form, this is the more general form, but it can be more difficult to process than the r_{ij} form. If the sampling intervals are consistent in the x- and y-directions of an *xyz* range image, it can be represented in the form of a large matrix of scaled, quantized range values r_{ij} where the corresponding x, y, z coordinates are determined implicitly by the row and column position in the matrix and the range value. The term "image" is used because any r_{ij} range image can be displayed on a video monitor, and it is identical in form to a digitized video image from a TV camera. The only difference is that pixel values represent distance in a range image whereas they represent irradiance (brightness) in a video image.

The term "large" in the definition above is relative, but for this survey, a range image must specify more than 100 (x, y, z) sample points. In Figure 1, the 20 × 20 matrix of heights of surface points above a plane is a small range image. If r_{ij} is the pixel value at the ith row and the jth column of the matrix, then the 3-D coordinates would be given as

$$x = a_x + s_x i \qquad y = a_y + s_y j \qquad z = a_z + s_z r_{ij} \quad (1)$$

where the s_x, s_y, s_z values are scale factors and the a_x, a_y, a_z values are coordinate offsets. This matrix of numbers is plotted as a surface viewed obliquely in Figure 2, interpolated and plotted as a contour map in Figure 3, and displayed as a black and white image in Figure 4. Each representation is an equally valid way to look at the data.

The affine transformation in equation (1) is appropriate for *orthographic* r_{ij} range images where depths are measured along parallel rays orthogonal to the image plane. Nonaffine transformations of (i, j, r_{ij}) coordinates to Cartesian (x, y, z) coordinates are more common in active optical range sensors. In the spherical coordinate system shown in Figure

171	160	163	163	166	166	168	166	168	166	163	160	163	163	160	163	166	163	166	163
168	166	166	163	166	163	168	166	166	166	163	163	166	163	166	163	166	160	163	163
168	168	166	166	166	163	160	166	166	171	166	168	168	166	160	163	166	160	160	166
166	163	166	166	163	163	160	163	179	174	185	177	185	179	212	196	185	204	196	185
163	166	160	166	163	163	166	190	174	168	168	182	185	190	201	196	199	182	196	199
166	163	163	163	168	160	163	166	166	163	168	177	190	188	199	188	190	196	193	185
163	166	166	157	160	160	160	171	160	168	168	182	199	199	199	193	199	188	193	193
160	160	160	166	157	160	168	166	166	163	163	182	201	199	190	188	190	190	193	193
163	166	157	163	160	157	160	177	166	160	171	201	215	199	196	201	190	190	188	188
155	160	160	163	160	163	160	166	166	163	163	204	207	207	190	185	193	190	196	196
157	155	163	160	157	157	168	166	168	163	177	188	201	199	196	196	201	182	210	196
157	157	155	157	160	157	163	171	163	157	155	204	185	196	193	188	196	188	193	201
157	160	155	155	157	157	168	168	163	166	166	190	201	201	196	188	190	193	185	193
157	155	160	160	157	157	163	157	157	160	157	182	204	190	185	190	190	188	185	188
157	157	157	160	157	157	152	166	160	163	166	193	196	193	199	190	190	185	190	185
155	157	160	160	160	152	166	152	163	152	168	171	212	212	193	190	188	182	188	185
152	157	155	155	152	155	149	163	160	155	157	185	210	210	212	215	210	185	204	193
155	155	157	152	152	155	155	171	174	166	171	188	188	199	188	204	188	185	215	207
155	157	152	157	149	157	157	168	179	204	182	221	174	193	182	179	212	188	201	182
155	155	155	155	152	149	146	174	188	193	168	185	168	179	171	190	190	193	190	179

Figure 1. 20 × 20 matrix of range measurements: r_{ij} form of range image.

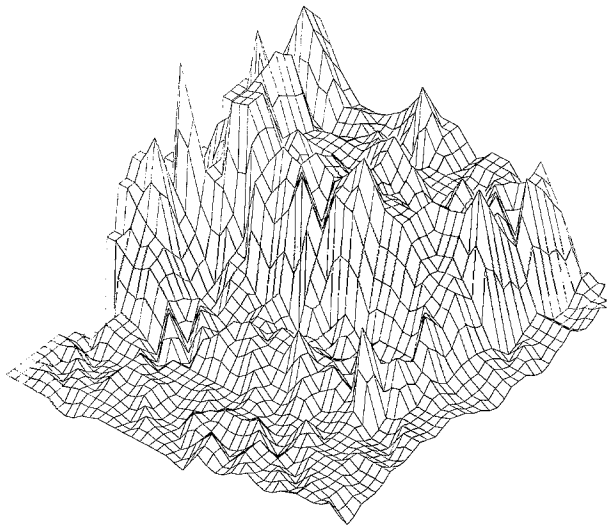

Figure 2. Surface plot of range image in Figure 1.

5, the (i, j) indices correspond to elevation (latitude) angles and azimuth (longitude) angles respectively. The spherical to Cartesian transformation is

$$\begin{aligned} x &= a_x + s_r r_{ij} \cos(is_\phi)\sin(js_\theta) \\ y &= a_y + s_r r_{ij} \sin(is_\phi) \\ z &= a_z + s_r r_{ij} \cos(is_\phi)\cos(js_\theta) \end{aligned} \quad (2)$$

where the s_r, s_ϕ, s_θ values are the scale factors in range, elevation, and azimuth and the a_x, a_y, a_z values are again the offsets. The "orthogonal-axis" angular coordinate system, also shown in Figure 5, uses an "alternate elevation angle" ψ with the spherical azimuth definition θ. The transformation to Cartesian coordinates is

$$\begin{aligned} x &= a_x + s_r r_{ij}\, tan(js_\theta)/\sqrt{1 + \tan^2(is_\theta) + \tan^2(js_\psi)} \\ y &= a_y + s_r r_{ij} \tan(is_\psi)/\sqrt{1 + \tan^2(is_\theta) + \tan^2(js_\psi)} \\ z &= a_z + s_r r_{ij}/\sqrt{1 + \tan^2(is_\theta) + \tan^2(js_\psi)}. \end{aligned} \quad (3)$$

The alternate elevation angle ψ depends only on y and z whereas ϕ depends on x, y, and z. The differences in (x, y, z) for equations (2) and (3) for the same values of azimuth and elevation are less than 4% in x and z and less than 11% in y, even when both angles are as large as ± 30 degrees.

2.1 Viewing Constraints and Motion Requirements

The first question in range imaging requirements is *viewing constraints*. Is a single view sufficient, or are multiple views of a scene necessary for the given application? What types of sensors are compatible with these needs? For example, a mobile robot can acquire data from its on-board sensors only at its current location. An automated modeling system may acquire multiple views of an object with many sensors located at different viewpoints. Four basic types of range sensors are distinguished based on the viewing constraints, scanning mechanisms, and object movement possibilities:

1. A *Point Sensor* measures the distance to a single visible surface point from a single viewpoint along a single ray. A point sensor can create a range image if (1) the scene object(s) can be physically moved in two directions in front of the point-ranging sensor, (2) if the point-ranging sensor can be scanned in two directions over the scene, or (3) the scene object(s) are stepped in

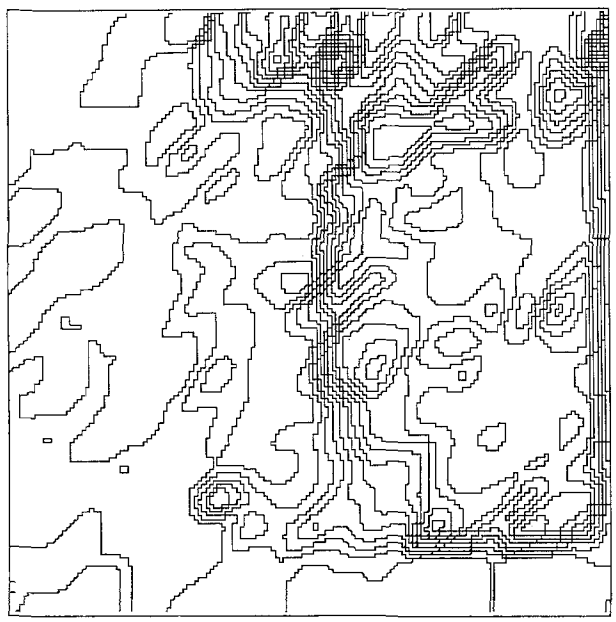

Figure 3. Contour plot of range image in Figure 1.

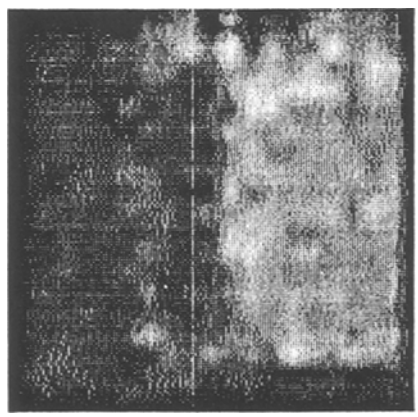

Figure 4. Gray level representation of range image in Figure 1.

one direction while the point sensor is scanned in the other direction.

2. A *Line* or *Circle Sensor* measures the distance to visible surface points that lie in a single 3-D plane or cone that contains the single viewpoint or viewing direction. A line or circle sensor can create a range image if (1) the scene object(s) can be moved orthogonal to the sensing plane or cone or (2) the line or circle sensor can be scanned over the scene in the orthogonal direction.
3. A *Field of View Sensor* measures the distance to many visible surface points that lie within a given field of view relative to a single viewpoint or viewing direction. This type of sensor creates a range image directly. No scene motion is required.
4. A *Multiple View Sensor System* locates surface points relative to more than one viewpoint or viewing direction because all surface points of interest are not visible or cannot be adequately measured from a single viewpoint or viewing direction. Scene motion is not required.

These sensor types form a natural hierarchy: a point sensor may be scanned (with respect to one sensor axis) to create a line or circle sensor, and a line or circle sensor may be scanned (with respect to the orthogonal sensor axis) to create a field of view sensor. Any combination of point, line/circle, and field of view sensors can be used to create a multiple view sensor by (1) rotating and/or translating the scene in front of the sensor(s); (2) maneuvering the sensor(s) around the scene with a robot; (3) using multiple sensors in different locations to capture the appropriate views; or any combination of the above.

Accurate sensor and/or scene object positioning is achieved via commercially available translation stages, $xy(z)$-tables, and $xy\theta$ tables (translation repeatability in submicron range, angular repeatability in microradians or arc-seconds). Such methods are preferred to mirror scanning methods for high precision applications because these mechanisms can be controlled better than scanning mirrors. Controlled 3-D motion of sensor(s) and/or object(s) via gantry, slider, and/or revolute joint robot arms is also possible, but is generally much more expensive than table motion for the same accuracy. Scanning motion internal to sensor housings is usually rotational (using a rotating mirror), but may also be translational (using a precision translation stage). Optical scanning of lasers has been achieved via (1) motor-driven rotating polygon mirrors, (2) galvanometer-driven flat mirrors, (3) acoustooptic (AO) modulators, (4) rotating holographic scanners, or (5) stepper-motor-driven mirrors (Gottlieb 1983, Marshall 1985). However, AO modulators and holographic scanners significantly attenuate laser power, and AO modulators have a narrow angular field of view ($\approx 10° \times 10°$), making them less desirable for many applications.

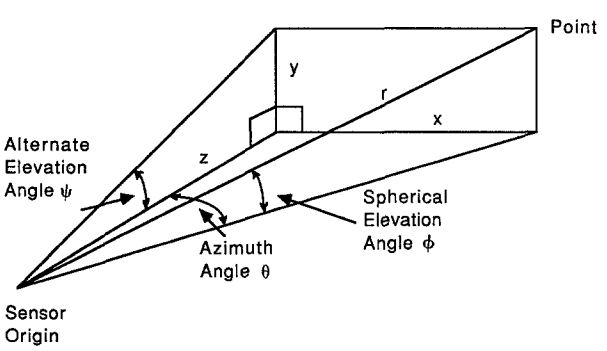

Figure 5. Cartesian, spherical, and orthogonal-axis coordinates.

2.2 Sensor Performance Parameters

Any measuring device is characterized by its measurement resolution or precision, repeatability, and accuracy. The following definitions are adopted here. *Range resolution* or *range precision* is the smallest change in range that a sensor can report. *Range repeatability* refers to statistical variations as a sensor makes repeated measurements of the exact same distance. *Range accuracy* refers to statistical variations as a sensor makes repeated measurements of a known *true value*. Accuracy should indicate the largest expected deviation of a measurement from the true value under normal operating conditions. Since range sensors can improve accuracy by averaging multiple measurements, accuracy should be quoted with measurement time. For our comparisons, a range sensor is characterized by its accuracy over a given measurement interval (the depth of field) and the measurement time. If a sensor has good repeatability, we assume that it is also calibrated to be accurate. Loss of calibration over time (drift) is a big problem for poorly engineered sensors but is not addressed here.

A range-imaging sensor measures point positions (x, y, z) within a specified accuracy or error tolerance. The method of specifying accuracy varies in different applications, but an accuracy specification should include one or more of the following for each 3-D direction given N observations: (1) the mean absolute error (MAE) $(\pm\delta_x, \pm\delta_y, \pm\delta_z)$ where $\delta_x = (1/N)\Sigma|x_i - \mu_x|$ and $\mu_x = (1/N)\Sigma x_i$ (or μ_x = median (x_i)); (2) RMS (root-mean-square) error $(\pm\sigma_x, \pm\sigma_y, \pm\sigma_z)$ where $\sigma_x^2 = (N-1)^{-1}\Sigma(x_i - \mu_x)^2$ and $\mu_x =$

$(1/N)\Sigma x_i$; or (3) maximum error ($\pm\epsilon_x$, $\pm\epsilon_y$, $\pm\epsilon_z$) where $\epsilon_x = \max_i|x_i - \mu_x|$. (Regardless of the measurement error probability distribution, $\delta \leq \sigma \leq \epsilon$ for each direction.) Some specify range accuracy (σ) with $\pm\sigma$ for RMS error as above; others specify $\pm 3\sigma$; others specify the positive width of the normal distribution as 2σ; and others do not say, if any of the above. Whatever specification is used, the sensor should ideally meet the specified error tolerance for any measured point within the working volume V of size $L_x \times L_y \times L_z$.

The foregoing parameters specify the spatial properties of the sensor. The pixel dwell time T is the time required for a single pixel range measurement. For points acquired *sequentially*, the total time to take N_p points in an image frame is N_pT, the frame rate is $1/N_pT$ frames/second, and the pixel data rate is $1/T$ pixels/second. If all points are acquired in *parallel* in time T, the frame rate is $1/T$ and the pixel rate N_p/T.

A system figure of merit maps several system parameters to a single number for comparing different systems. An application independent performance figure of merit M is defined to measure the spatial and temporal performance of range imaging sensors. For xyz-form range imaging, the figure of merit M is defined as

$$M = \frac{1}{\sqrt{T}}\left(\frac{L_xL_yL_z}{\sigma_x\sigma_y\sigma_z}\right)^{1/3}. \tag{4}$$

For r_{ij}-form range imaging, there is usually very little relative uncertainty in the direction of a ray specified by the interger i and j indices compared to the uncertainty in the measured range r. Thus, the uncertainty in the resulting x, y, z coordinates is dominated by the uncertainty in the r_{ij} values. The working volume is a portion of a pyramid cut out by spherical surfaces with the minimum and maximum distance radii. The figure of merit for r_{ij}-form range-imaging sensors is given by the simpler expression

$$M \approx \frac{L_r}{\sigma_r\sqrt{T}} \tag{5}$$

where L_r is the *depth of field* and σ_r is the *RMS range accuracy*. Both quantities are defined along rays emanating from the sensor. The factors of standoff distance, angular field of view, and field of view are other important parameters for range sensors that do not enter into the figure of merit calculations directly, but should be considered for each application. These parameters are shown in Figure 6.

The dimensions of M may be thought of roughly as the amount of good quality range data per second, and of course, the higher the number the better, other things being equal. A doubling of the depth-of-field to range-accuracy ratio is reflected by a doubling of the figure of merit. However, a quadrupling of image acquisition speed is required to double the figure of merit. This expresses a bias for accurate measurement over fast measurement, but also maintains an invariant figure of merit under internal sensor averaging changes. Suppose a system does internal averaging of normally distributed measurement errors during the pixel dwell time T. If T is quartered, the σ-value should only double. If the square root of time T were not used, the figure of merit would double as the data became noisier and the sensor got faster. This was considered undesirable.

The figures of merit quoted in this survey should be taken as examples of the rough order of magnitude of sensor performance, not exact numbers. First, it is difficult to know the actual accuracy for a given application without testing a sensor on typical scenes. Second, it is difficult to know whether quoted accuracy means 1, 2, 3, or 4σ or something else. Third, even if the quoted figure is a valid test result, the surface reflectance, absorption, and transmission properties for the test are not always stated. Sensor performance is often quoted under the most favorable conditions. Fourth, several sensors, especially sensors from conservative commercial companies, are underrated because of conservative accuracy figures. They know about the vast difference between measurements in the lab and in the customer's plant and about customer disappointment. In fact, some sensors are conservatively rated 10 to 20 times less accurate than they would be in the lab. Finally, only resolution is given for some sensors and accuracy had to be estimated.

The sensor cost C can be combined with the performance figure of merit to create a cost-weighted

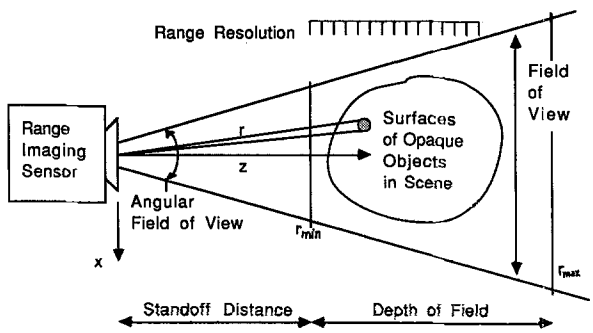

Figure 6. Range imaging sensor with angular scan.

figure of merit $M' = M/C$ where the dimensions are roughly range data per second per unit cost. Cost estimates are not included here because actual costs can vary significantly from year to year depending upon technical developments and market forces, not to mention customized features that are often needed for applications. Cost estimates were also not available for many sensors.

It is likely that these figures of merit M and M' may place no importance on factors that dominate decisions for a particular application. The figures of merit given here are application independent. No figure of merit can represent all factors for all applications. For example, some triangulation or moire range sensors with large source/detector separations may have a significant "missing parts" problem (shadowing problem) for certain applications and not for others. Figures of merit cannot easily reflect this limitation.

Neither can the "scene materials" problem be easily factored into a figure of merit. There are materials in many scenes that almost completely reflect, absorb, or transmit optical radiation. For example, mirrors and shiny metal or plastic surfaces reflect light, black paint may absorb infrared, and glass is transparent. These materials cause scene geometry interpretation problems for optical sensors. Hence, the physical/chemical composition of matter in a scene determines the quality and the meaning of range values. Even though optical range sensors are designed for determining scene geometry directly, a priori information about the optical properties of scene materials is needed for accurate interpretation.

3. Imaging Radars

Bats (Griffin 1958) and porpoises (Kellogg 1961) are equipped by nature with ultrasonic "radars." Electromagnetic radar dates back to 1903 when Hulsmeyer (1904) experimented with the detection of radio waves reflected from ships. The basic time/range equation for radars is

$$v\tau = 2r = \text{round-trip distance} \tag{6}$$

where v is the speed of signal propagation, r is the distance to a reflecting object, and τ is the transit time of the signal traveling from the radar transmitter to the reflecting object and back to the radar receiver. For imaging laser radars, the unknown scene parameters at a reflecting point are the (1) range r, (2) the surface reflection coefficient (albedo) ρ, and (3) the angle $\theta = \cos^{-1}(\hat{n} \cdot \hat{l})$ between the visible surface normal $\hat{n}$ and the direction $\hat{l}$ of the radar beam. Ignoring atmospheric attenuation, all other relevant physical parameters can be lumped into a single function $K(t)$ that depends only on the radar transceiver hardware. The received power $P(t)$ is

$$P(t, \theta, \rho, r) = K(t - \tau)\rho \cos\theta / r^2 \tag{7}$$

This laser radar equation tells us that if 10 bits of range resolution are required on surfaces that may tilt away from the sight line by as much as 60 deg, and if surface reflection coefficients from 1 to 0.002 are possible on scene surfaces, then a radar receiver with a dynamic range of 90 dB is required.

3.1 Time of Flight, Pulse Detection

In this section, several pulse detection imaging laser radars are mentioned. A figure of merit M is assigned to each sensor.

Lewis and Johnston at JPL built an imaging laser radar beginning in 1972 for the Mars rover (Lewis and Johnston 1977). Their best range resolution was 20 mm over a 3-m depth of field and the maximum data rate possible was 100 points per second. It took about 40 seconds to obtain 64 × 64 range images (M = 1520).

Jarvis (1983a) built a similar sensor capable of acquiring a 64 × 64 range image with ±2.5 mm range resolution over a 4 m field of view in 40 s (M = 16,160).

Heikkinen et al. (1986) and Ahola et al. (1985) developed a pulsed time-of-flight range sensor with a depth of field of 1.5 m at a standoff of 2.5 m. The range resolution is about 20 mm at its maximum data rate (10,000 points/s) at a range of 3.5 m (M = 7500).

Ross (1978) patented a novel pulsed, time-of-flight imaging laser radar concept that uses several fast camera shutters instead of mechanical scanning. For a range sensor with 30 cm resolution over a 75-m depth of field, the least significant range-bit image is determined by a 2-ns shutter (the fastest shutter required). Assuming a conservative frame rate of 15 Hz and eight, 512 × 512 cameras, M = 500,000 if constructed.

An imaging laser radar is commercially available for airborne hydrographic surveying (Banic et al. 1987). The system can measure water depths down to 40 m with an accuracy of 0.3 m from an aerial standoff of 500 m. Two hundred scan lines were acquired covering 2000 km^2 with two million

"soundings" in 30 h (M = 596). This number is low because *application specific capabilities* (e.g., standoff) are not included.

3.2 Amplitude Modulation

Rather than sending out a short pulse, waiting for an echo, and measuring transit time, a laser beam can be amplitude-modulated by varying the drive current of a laser diode at a frequency $f_{AM} = c/\lambda_{AM}$. An electronic phase detector measures the phase difference $\Delta\phi$ (in radians) between the transmitted signal and the received signal to get the range: $r(\Delta\phi) = c\Delta\phi/4\pi f_{AM} = \lambda_{AM}\Delta\phi/4\pi$. Since relative phase differences are only determined modulo 2π, the range to a point is only determined within a range ambiguity interval r_{ambig}. In the absence of any ambiguity-resolving mechanisms, the depth of field of an AM laser radar is the ambiguity interval: $L_r = r_{ambig} = c/2f_{AM} = \lambda_{AM}/2$ which is divided into $2^{N_{bits}}$ range levels where N_{bits} is the number of bits of quantization at the output of the phase detector. Finer depth resolution and smaller ambiguity intervals result from using higher modulating frequencies.

The ambiguity interval problem in AM CW radars can be resolved either via software or more hardware. If the imaged scene is limited in surface gradient relative to the sensor, it is possible in software to unwrap phase ambiguities because the phase gradient will always exceed the surface gradient limit at phase wraparound pixels. This type of processing is done routinely in moire sensors (see Halioua and Srinivasan 1987). In hardware, a system could use multiple modulation frequencies simultaneously. In a simple approach, each range ambiguity is resolved by checking against lower modulation frequency measurements. Other methods are possible, but none are commercially available at the current time.

Nitzan et al. (1977) built one of the first nonmilitary AM imaging laser radars. It created high-quality registered range and intensity images. With a 40-dB signal-to-noise ratio (SNR), a range accuracy of 4 cm in an ambiguity interval of 16.6 m was obtained. With a 67 dB SNR, the accuracy improved to 2 mm. The pixel dwell time was variable: 500 ms per pixel dwell times were common and more than 2 h was needed for a full 128 × 128 image (M = 3770 at 67 dB). The system insured image quality by averaging the received signal until the SNR was high enough.

The Environmental Research Institute of Michigan (ERIM) developed three AM imaging laser radars: (1) the Adaptive Suspension Vehicle (ASV) system, (2) the Autonomous Land Vehicle (ALV) system, and (3) the Intelligent Task Automation (ITA) system. Zuk and Dell'Eva (1983) described the ASV sensor. The range accuracy is about 61 mm over 9.75 m at a frame rate of two 128 × 128 images per second (M = 28,930). The ALV sensor generates two 256 × 64 image frames per second. The ambiguity interval was increased to 19.5 m, but M = 28930 is identical to the ASV sensor since pixel dwell time and depth of field to range accuracy ratios stayed the same. The new ERIM navigation sensor (Sampson 1987) uses lasers with three different frequencies and has 2-cm range resolution (M = 353,000 assuming depth of field is doubled). The ERIM ITA sensor is programmable for up to 512 × 512 range images (Svetkoff et al. 1984). The depth of field can change from 150 mm to 900 mm. As an inspection sensor, the laser diode is modulated at 720 MHz. The sensor then has a range accuracy of 100 μ at a standoff of 230 mm in a 76-mm × 76-mm field of view over a depth of field of 200 mm. The latest system of this type claims a 100-kHz pixel rate (M = 632,500).

A commercially available AM imaging laser radar is built by Odetics (Binger and Harris 1987). Their sensor has a 9.4-m ambiguity interval with 9-bit range resolution of 18 mm per depth level. The pixel dwell time is 32 μsec (M = 71,720). This sensor features an *auto-calibration feature* that calibrates the system *every frame* avoiding thermal drift problems encountered in other sensors of this type. It is currently the smallest (9 × 9 × 9 in.), lightest weight (33 lbs.), and least power hungry (42 W) sensor in its class. Class I CDRH eye safety requirements (see the appendix) are met except within a 0.4 m radius of the aperture.

Another commercially available AM imaging laser radar is built by Boulder Electro-Optics (1986). The ambiguity interval is 43 m with 8-bit resolution (about 170 mm). The frame rate was 1.4 256 × 256 frames/sec (M = 27,360).

Perceptron (1987) reports they are developing an AM imaging laser radar with a 360-kHz data rate, a 1.87-m ambiguity interval, a 3-m standoff, and 0.45-mm (12-bit) range resolution (M = 153,600 assuming 8-bit accuracy).

Cathey and Davis (1986) designed a system using multiple laser diodes, one for each pixel, to avoid scanning. They obtained a 15-cm range accuracy at a range of 13 m with a 2-diode system. For N^2 laser diodes fired four times a second, $M = 512N$. If the sensor cost is dominated by N^2 laser diode cost, the cost-weighted figure of merit M' would decrease as $1/N$. A full imaging system has not been built.

Miller and Wagner (1987) built an AM radar unit using a modulated infrared LED. The system scans 360 deg in azimuth, digitizing about 1000 points in a second. The depth of field is about 6 m with a range accuracy of about 25 mm (M = 7590). This system is very inexpensive to build and is designed for mobile robot navigation.

The Perkin-Elmer imaging airborne laser radar (Keyes 1986) scans 2790 pixels per scan line in 2 ms (M = 302,360 assuming 8-bit range accuracy). Aircraft motion provides the necessary scanning motion in the flight direction of the aircraft.

Wang et al. (1984) and Terras (1986) discussed the imaging laser radar developed at General Dynamics. The 12 × 12-deg angular field of view is scanned by dual galvanometers. It ranges out to 350 m, but the ambiguity interval is 10 m yielding lots of phase transition stripes in uncorrected range images.

Other work in AM imaging laser radars has been done at Hughes Aircraft, MIT Lincoln Labs (Quist et al. 1978), Raytheon (Jelalian and McManus 1977), as well as United Technologies and other defense contractors.

3.3 Frequency Modulation, Heterodyne Detection

The optical frequency of a laser diode can also be tuned thermally by modulating the laser diode drive current (Dandridge 1982). If the transmitted optical frequency is repetitively swept linearly between $\nu \pm \Delta\nu/2$ to create a total frequency deviation of $\Delta\nu$ during the period $1/f_m$ (f_m is the linear sweep modulation frequency), the reflected return signal can be mixed coherently with a reference signal at the detector (Teich 1968) to create a beat frequency f_b signal that depends on the range to the object r (Skolnick 1962). This detection process is known as FM coherent heterodyne detection. Range is proportional to the beat frequency in an FM CW radar: $r(f_b) = cf_b/4f_m\Delta\nu$. One method for measuring the beat frequency is counting the number of zero-crossings N_b of the beat signal during a ramp of the linear sweep frequency modulation. This zero-crossing count must satisfy the relationship $2N_b = \lfloor f_b/f_m \rfloor$ which yields the range equation $r(N_b) = cN_b/2\Delta\nu$. The range values in this method are determined to within $\delta r = \pm c/4\Delta\nu$ since N_b must be an integer. The maximum range should satisfy the constraint that $r_{max} \ll c/f_m$. Since it is difficult to ensure the exact optical frequency deviation $\Delta\nu$ of a laser diode, it is possible to measure range indirectly by comparing the N_b value with a known reference count N_{ref} for an accurately known reference distance r_{ref} using the relationship $r(N_b) = N_b r_{ref}/N_{ref}$. Hersman et al. (1987) reported results for two commercially available FM imaging laser radars: a vision system and a metrology system (Digital Optronics 1986). The vision system measures a 1-m depth of field with 8-bit resolution at four 256 × 256 frames/second (M = 3770 using a quoted value of 12 mm for RMS depth accuracy after averaging 128 frames in 32 s). A new receiver is being developed to obtain similar performance in 0.25 s. The metrology system measures to an accuracy of 50 μ in 0.1 s over a depth of field of 2.5 m (M = 30,430). Better performance is expected when electronically tunable laser diodes are available.

Beheim and Fritsch (1986) reported results with an in-house sensor. Points were acquired at a rate of 29.3/s. The range accuracy varied with target to source distance. From 50 to 500 mm, the range accuracy was 2.7 mm; from 600 to 1000 mm, σ_z = 7.4 mm; and from 1100 to 1500 mm, σ_z = 15 mm (approximately M = 1080).

4. Active Triangulation

Triangulation based on the law of sines is certainly the oldest method for measuring range to remote points and is also the most common. A simple geometry for an active triangulation system is shown in Figure 7. A single camera is aligned along the z-axis with the center of the lens located at (0, 0, 0). At a baseline distance b to the left of the camera (along the negative x-axis) is a light projector sending out a beam or plane of light at a variable angle θ relative to the x-axis baseline. The point (x, y, z) is projected into the digitized image at the pixel (u, v) so $uz = xf$ and $vz = yf$ by similar triangles where f is the focal length of the camera in pixels. The measured quantities (u, v, θ) are used to compute the (x, y, z) coordinates:

$$[x\ y\ z] = \frac{b}{f\cot\theta - u}[u\ v\ f] \tag{8}$$

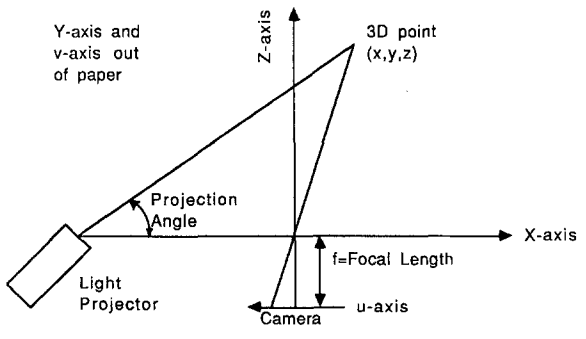

Figure 7. Camera-centered active triangulation geometry.

4.1 Structured Light: Point

It is commonly believed that a large baseline distance b separating the light source and the detector is necessary for accurate ranging. However, for any fixed focal length f and baseline distance b, the range resolution of a triangulation system is only limited by the ability to accurately measure the angle θ and the horizontal position u.

Rioux (1984) has patented a synchronized scanner concept for active triangulation in which the horizontal position detector and the beam projector are *both* scanned. The angle θ is coupled with the u measurement yielding high-range resolution with a small baseline by making more efficient use of the finite resolution of the horizontal position detector. The basic concept is that if one uses the available resolution to measure differences from the mean rather than absolute quantities, the effective resolution can be much greater. As shown in Figure 8, the beam leaves the source, hits the mirror currently rotated at a position θ, bounces off a fixed (source) mirror and impinges on an object surface. The illuminated bright spot is viewed via the opposite side of the mirror (and a symmetrically positioned fixed detector mirror). The average range is determined by the angular positioning of the fixed mirrors. The sensor creates a 128 × 256 range image in less than a second. The angular separation of the fixed mirrors is only 10 deg. For a total working volume of 250 mm × 250 mm × 100 mm, the x, y, z resolutions are 1, 2, and 0.4 mm, respectively (M = 45,255).

Servo-Robot (1987) manufactures the Saturn and the Jupiter line scan range sensors. Both are based on synchronous scanning. The Saturn system measures a 60 mm × 60 mm × 60 mm working volume from a standoff of 80 mm. The volume-center resolution is 0.06 mm in x and 0.05 mm in z (M = 32,860 for 3000 points/s). The Jupiter system measures a 1 m × 1 m × 1 m volume from a standoff of 0.1 m. The volume-center resolution is 1 mm in x and 0.3 mm in z (M = 91,290 for 3000 points/s).

Hymarc (1987) also makes a line scan sensor based on synchronous scanning. The sensor is accurate to 0.25 mm in a 500 mm × 500 mm × 500 mm working volume at a 600-mm standoff with a 3000 point per second data rate (M = 109,540).

Photonic Automation, Inc. (1987) is developing a commercially available sensor for fast ranging in a shallow depth of field. They claim a range accuracy of 25 μ over a depth of field of 6.25 mm at a speed of 10 million pixels per second (M = 790,570). The angular separation between source and detector is about 5 deg. Synthetic Vision Systems of Ann Arbor, Michigan has a competing unit.

Bickel et al. (1984) independently developed a mechanically coupled deflector arrangement for spot scanners similar in concept to the Rioux (1984) design. Bickel et al. (1985) addressed depth of focus problems inherent in triangulation systems for both illumination and detection. They suggest a teleaxicon lens and a laser source can provide a 25-μ spot that is in focus over a 100-mm range at a 500-mm standoff. Detection optics should be configured to satisfy the Scheimpflug (tilted detector plane) condition (Slevogt 1974) shown in Figure 9: $\tan \theta_{tilt} = 1/M \tan \theta_{sep}$ where θ_{sep} is the separation angle of the illumination direction and the detector's viewing direction, θ_{tilt} is the tilt angle of the photosensitive surface in the focusing region of the lens relative to the viewing direction, and $M = (w_c - f)/w_c$ is the on-axis magnification of the lens where w_c is the distance from the center of the lens to the center of the detector plane and f is the focal length of the lens. All points in the illumination plane are in exact focus in the detector plane. Using a 4000-element linear array detector, they get 25-μ range resolution, 13-μ lateral resolution, over a depth of field of 80 mm (M = 17,530 assuming 30 points/s rate). Tilted detector planes are used by some commercial

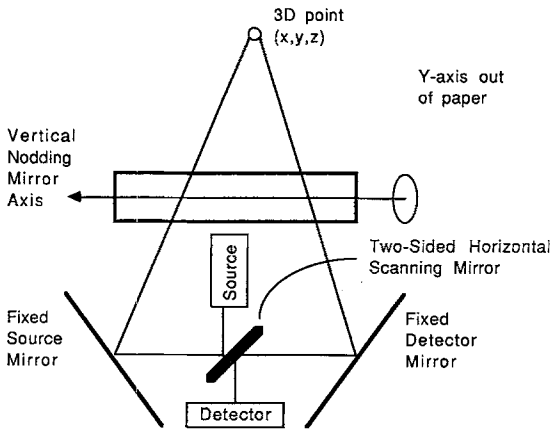

Figure 8. Synchronous scanning of source and detector.

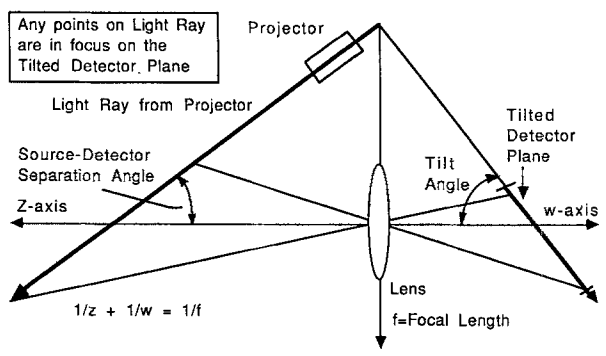

Figure 9. Scheimpflug condition: tilted detector to maintain focus for all depths.

vendors. Hausler and Maul (1985) examined the use of telecentric scanning configurations for point scanners. A telecentric system positions optical components at the focal length of the lens (or mirror).

Faugeras and Hebert (1986) used an in-house laser scanner. Their sensor uses a laser spot projector and two horizontal position detectors. Objects are placed on a turntable, and points are digitized as the object rotates. Scans are taken at several different heights to define object shape. No numbers were available to compute the figure of merit.

CyberOptics Corp. (1987) manufactures a series of point range sensors. For example, the PRS-30 measures a 300 μ depth of field from a standoff of 5 mm with 0.75-μ accuracy (1 part in 400). A precision xy-table (0.25 μ) provides object scanning under a stationary sensor at a rate of 15 points/s (M = 1550).

Diffracto, Ltd. (1987) also makes a series of point range sensors. Their Model 300 LaserProbe measures a depth of field of 2 mm from a standoff of 50 mm with an accuracy of 2.5 μ in 5 ms (M = 11,300). The detector handles a 50,000:1 dynamic range of reflected light intensities and works well for a variety of surfaces.

Kern Instruments (1987) has developed the System for Positioning and Automated Coordinate Evaluation (SPACE) using two automated Kern theodolites. This system measures points in a 3 m × 3 m × 3 m working volume to an accuracy of 50 μ (1 part in 60,000) at a rate of about 7.5 s per point (M = 21,910).

Lorenz (1984, 1986) has designed an optical probe to measure range with a repeatability of 2.5 μ over a depth of field of 100 mm (1 part in 40,000). He uses split-beam illumination and optimal estimation theory. The probe was tested on the z-axis of a CNC machining center. Even at one point per second, M = 40000.

The Selcom Opticator (1987) series are among the highest performance commercially available ranging point probes. They measure with one part in 4000 resolution at 16,000 points/s (M = 126,490 for 1 part in 1000 accuracy). The resolution of different models ranges from 2 to 128 μ in powers of two.

Pipitone and Marshall (1983) documented their experience in building a point scanning system. They measured with an accuracy of about 1 part in 400 over a depth of field of about 7.6 m (M = 8940 for 500 pts/s).

Haggren and Leikas (1987) have developed a four-camera photogrammetric machine-vision system with accuracy of better than 1 part in 10,000. The system generates one 3-D point every 1.5 s (M = 8160). Earlier similar photogrammetry work is found in Pinckney (1978) and Kratky (1979).

4.2 Structured Light: Line

Passing a laser beam through a cylindrical lens creates a line of light. Shirai (1972) and Will and Pennington (1972) were some of the first researchers to use light striping for computer vision. Nevatia and Binford (1973), Rocker (1974), and Popplestone et al. (1975) also used light striping. The General Motors Consight System (Holland et al. 1979) was one of the first industrial systems to use light stripe principles.

Technical Arts Corp. (1987) produces the 100X White Scanner. The camera and laser are typically separated by 45 deg or more. The system can measure up to a range of 2.4 m with a resolution of about 0.5 mm (M = 87,640 for 3000 pts/s and accuracy of 1.5 mm).

The IMAGE Lab at ENST in France developed a light stripe laser ranging system (Schmitt et al. 1985), commercially available from Studec. Schmitt et al. (1986) show a range image of a human head sculpture obtained with this sensor.

Cotter and Batchelor (1986) describe a depth map module (DMM) based on light striping techniques that produces 128 × 128 range images in about 4 s (M = 8192 assuming 7-bit resolution).

Silvaggi et al. (1986) describe a very inexpensive triangulation system (less than $1000 in component cost) that is accurate to 0.25 mm over a 50-mm depth of field at a standoff of 100 mm. A photosensitive RAM chip is used as the camera.

CyberOptics Corp. (1987) also manufactures a series of line range sensors. The LRS-30-500 measures a 300 μ depth of field and an 800-μ field of view from a standoff of 15 mm with 0.75 μ range accuracy (1 part in 400). A precision xy-table (0.25 μ) provides object scanning under the stationary sensor head at a rate of 5 lines/s (M = 7155 assuming only 64 points per line).

Perceptron (1987) makes a contour sensor that uses light striping and the Scheimpflug condition to obtain 25-μ accuracy over a 45-mm depth of field at a rate of 15 points/s (M = 6970).

Diffracto, Ltd. (1987) manufactures a Z-Sensor series of light stripe range sensors. Their Z-750 can measure a 19 mm depth of field with an accuracy of 50 μ from a standoff of 762 mm (M = 6100 assuming one 256 point line/s).

Landman and Robertson (1986) describe the capabilities of the Eyecrometer system available from Octek. This system is capable of 25 μ 3σ accuracy in the narrow view mode with a 12.7 mm depth

of field. The time for a high-accuracy scan is 9.2 s (M = 2680 assuming 256 pixels/scan).

Harding and Goodson (1986) implemented a prototype optical guillotine system that uses a high-precision translation stage with 2-μ resolution to obtain an accuracy of 1 part in 16,000 over a range of 150 mm. The system generates a scan in about 1 s (M = 256,000 assuming a 256-point scan).

The APOMS (Automated Propeller Optical Measurement System) built by RVSI (Robotic Vision Systems, Inc.) (1987) uses a high precision point range sensor mounted on the arm of a 5-axis inspection robot arm. The large working volume is 3.2 m $\times$ 3.5 m $\times$ 4.2 m. The accuracy of the optical sensor (x, y, z) coordinates is 64 μ in an 81 mm $\times$ 81 mm field of view. The linear axes of the robot are accurate to 2.5 μ, and the pitch and roll axes are accurate to 2 arc-seconds. The system covers 60 square feet per hour. Assuming 4 points per square millimeter, the data rate is about 6000 points/s (M = 3,485,700). The RVSI Ship Surface Scanner is a portable tripod mounted unit that has a maximum 70 deg $\times$ 70 deg field of view. The line scanner scans at an azimuthal rate of 8 deg/s. The range accuracy is about 1 part in 600 or about 5.7 mm at 3.66 m. The RVSI RoboLocator sensor can measure depths to an accuracy of 50 μ in a 25 mm $\times$ 25 mm field of view and a 50 mm depth of field. The RVSI RoboSensor measures about 1 part in 1000 over up to a 1-m depth of field in a 500 mm $\times$ 500 mm field of view. Assuming 3000 points/s, M = 54,000.

4.3 Structured Light: Miscellaneous

Kanade and Fuhrman (1987) developed an 18 LED light-source optical proximity sensor that computes 200 local surface points in 1 s with a precision of 0.1 mm over a depth of field of 100 mm (M = 14,140). Damm (1987) has developed a similar but smaller proximity sensor using optical fibers.

Labuz and McVey (1986) developed a ranging method based on tracking the multiple points of a moving grid over a scene. Lewis and Sopwith (1986) used the multiple-point-projection approach with a static stereo pair of images.

Jalkio et al. (1985) use multiple light stripes to obtain range images. The field of view is 60 mm $\times$ 60 mm with at least a 25-mm depth of field. The range resolution is about 0.25 mm with a lateral sampling interval of 0.5 mm. The image acquisition time was dominated by software processing of 2 min (M = 1170).

Mundy and Porter (1987) describe a system designed to yield 25-μ range resolution within 50 μ $\times$ 50 μ pixels at a pixel rate of 1 MHz while tolerating a 10 to 1 change in surface reflectance. The goals were met except the data acquisition speed is about 16 kHz (M = 32,380 assuming 8-bit accuracy).

Range measurements can be extracted from a single projected grid image, but if no constraints are imposed on the surface shapes in the scene, ambiguities may arise. Will and Pennington (1972) discussed grid-coding methods for isolating planar surfaces in scenes based on vertical and horizontal spatial frequency analysis. Hall et al. (1982) described a grid-pattern method for obtaining sparse range images of simple objects. Potmesil (1983) used a projected grid method to obtain range data for automatically generating surface models of solid objects. Stockman and Hu (1986) examined the ambiguity problem using relaxation labeling. Wang et al. (1985) used projected grids to obtain local surface orientation.

Wei and Gini (1983) proposed a structured light method using circles. They propose a spinning mirror assembly to create a converging cone of light that projects to a circle on a flat surface and an ellipse on a sloped surface. Ellipse parameters determine the distance to the surface as well as the surface normal (within a sign ambiguity).

If the light source projects two intersecting lines (X), it is easier to achieve subpixel accuracy at the point. The cross is created by a laser by using a beamsplitter and two cylindrical lenses. Pelowski (1986) discusses a commercially available Perceptron sensor that guarantees a $\pm 3\sigma$ accuracy in (x, y, z) of 0.1 mm over a depth of field of 45 mm in less than 0.25 s. Nakagawa and Ninomiya (1987) also uses the cross structure.

Asada et al. (1986) project thick stripes to obtain from a single image a denser map of surface normals than is possible using grid projection. The thickness of the stripes limits ambiguity somewhat because of the signed brightness transitions at thick stripe edges.

4.4 Structured Light: Coded Binary Patterns

Rather than scan a light stripe over a scene and process N separate images or deal with the ambiguities possible in processing a single gray scale multistripe image, it is possible to compute a range image using $N' = \top \log_2 N \top$ images where the scene is illuminated with binary stripe patterns. In an appropriate configuration, a range image can be computed from intensity images using lookup tables. This method is fast and relatively inexpensive.

Solid Photography, Inc. (1977) made the first use of gray-coded binary patterns for range imaging. A gantry mounted system of several range cameras acquired range data from a 2π solid angle around an

object. The system was equipped with a milling machine so that if a person had his or her range picture taken, a 3-D bust could be machined in a matter of minutes. The point accuracy of the multisensor system was about 0.75 mm in a 300 mm × 300 mm × 300 mm volume (M = 100,000 assuming 64K points/s).

Altschuler et al. (1981) and Potsdamer and Altschuler (1983) developed a numerical stereo camera consisting of a laser and an electrooptic shutter synchronized to a video camera. They used standard binary patterns and also performed experiments using two crossed electrooptic shutters (grid-patterns).

Inokuchi et al. (1984) and Sato and Inokuchi (1985) showed results from their system based on the gray-code binary pattern concept. More recently, Yamamoto et al. (1986) reported another approach based on binary image accumulation. A variation on the binary pattern scheme is given in Yeung and Lawrence (1986).

Rosenfeld and Tsikos (1986) built a range camera using 10 gray-code patterns on a 6-in. dia disk that rotates at 5 revolutions per second. Their system creates a 256 × 256 8-bit range image with 2-mm resolution in about 0.7 s (M = 78,330).

Vuylsteke and Oosterlinck (1986) developed another binary coding scheme. They use a projection of a specially formulated binary mask where each local neighborhood of the mask has its own signature. A 64 × 64 range image was computed from a 604 × 576 resolution intensity image in about 70 CPU s (VAX 11/750) (M = 1260 assuming 7-bit accuracy).

4.5 Structured Light: Color Coded Stripes

Boyer and Kak (1987) developed a real-time light striping concept that requires only one image frame from a color camera (no mechanical operations). If many stripes are used to illuminate a scene and only one monochrome image is used, ambiguities arise at depth discontinuities because it is not clear which image stripe corresponds to which projected stripe. However, when stripes are color coded, unique color subsequences can be used to establish the correct correspondence for all stripes. Although no figures are given, 128 × 128 images with 8-bit accuracy at a 7.5-Hz frame rate would yield M = 89,000.

4.6 Structured Light: Intensity Ratio Sensor

The intensity ratio method, invented by Schwartz (1983), prototyped by Bastuschek and Schwartz (1984), researched by Carrihill (1986), and documented by Carrihill and Hummel (1985), determines range unambiguously using the digitization and analysis of only three images: an ambient image, a projector-illuminated image, and a projected lateral attenuation filter image. The depth of field was 860 mm with a range resolution of 12 bits at a standoff of 80 cm, but an overall range repeatability of 2 mm. The total acquisition and computation time for a 512 × 480 image with a Vicom processor was about 40 s (M = 33,700).

4.7 Structured Light: Random Texture

Schewe and Forstner (1986) developed a precision photogrammetry system based on random texture projection. A scene is illuminated by a texture projector and photographed with stereo metric cameras onto high-resolution glass plates. Registered pairs of subimages are digitized from the plates, and a manually selected starting point initializes automated processing. The range accuracy of the points is about 0.1 mm over about a 1-m depth of field and a several-meter field of view. A complete wireframe model is created requiring a few seconds per point on a microcomputer (M = 10,000).

5. Moire Techniques

A moire pattern is a low spatial frequency interference pattern created when two gratings with regularly spaced patterns of higher spatial frequency are superimposed on one another. Mathematically, the interference pattern $A(x)$ from two patterns A_1, A_2 is

$$A(x) = A_1\{1 + m_1 \cos[\omega_1 x + \phi_1(x)]\} \cdot A_2\{1 + m_2 \cos[\omega_2 x + \phi_2(x)]\} \quad (9)$$

where the A_i are amplitudes, the m_i are modulation indices, the ω_i are spatial frequencies, and the $\phi_i(x)$ are spatial phases. When this signal is low-pass filtered (LPF) (blurred), only the difference frequency and constant terms are passed:

$$A'(x) = \mathrm{LPF}[A(x)] = A_1A_2(1 + m_1m_2 \cos\{[\omega_1 - \omega_2)x + \phi_1(x) - \phi_2(x)]\}. \quad (10)$$

For equal spatial frequencies, only the phase difference term remains. In moire range-imaging sensors, surface depth information is encoded in and recovered from the phase difference term. Reviews and bibliographies of moire methods may be found in Pirodda (1982), Sciammarella (1982), and Oster (1965). Theocaris (1969) provides some history of moire techniques (e.g., Lord Rayleigh 1874).

Moire range-imaging methods are useful for measuring the *relative distance* to surface points on a smooth surface $z(x, y)$ that does not exhibit depth

discontinuities. The magnitude of surface slope as viewed from the sensor direction should be bounded $\|\nabla z\| < K$. Under such constraints, absolute range for an entire moire image can be determined if the distance to one reference image point is known.

Moire methods for surface measurement use line gratings of alternating opaque and transparent bars of equal width (Ronchi gratings). The *pitch* P of a grating is the number of opaque/transparent line-pairs per millimeter (LP/mm). The period $p = 1/P$ of the grating is the distance between the centers of two opaque lines.

5.1 Projection Moire

Khetan (1975) gives a theoretical analysis of projection moire. In a projection moire system, a precisely matched pair of gratings is required. The projector grating is placed in front of the projector and the camera grating is placed in front of the camera as shown in Figure 10. The projector is located at an angle θ_l and the camera is located at an angle θ_v relative to the z-axis. The projected light is spatially amplitude modulated by the pitch of the projector grating, creating a spatial "carrier" image. When the projected beam falls on the smooth surface, the surface shape modulates the phase of the spatial carrier. By viewing these stripes through the camera grating, interference fringes are created at the camera. The camera grating "demodulates" the modulated carrier yielding a "baseband" image signal whose fringes carry information about surface shape. If p_o is the period of the projected fringes at the object surface, then the change in z between the centers of the interference fringes viewed by the camera is given by

$$\Delta z = \frac{p_o}{\tan(\theta_l) + \tan(\theta_v)}. \tag{11}$$

The angular separation of source and detector is critical to range measurement and thus, moire may be considered a triangulation method (Perrin and Thomas 1979).

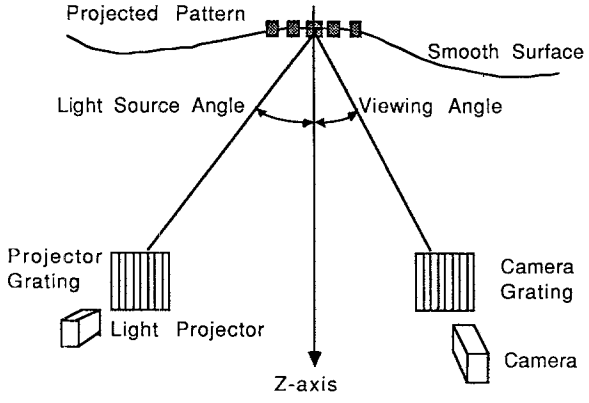

Figure 10. Projection moire configuration.

It is relatively inexpensive to set up a moire system using commercially available moire projectors, moire viewers, matched gratings, and video cameras (Newport Corp. 1987). The problem is accurate calibration and automated analysis of moire fringe images. Automated fringe analysis systems are surveyed in Reid (1986). The limitations of projection moire automated by digital image processing algorithms are addressed by Gasvik (1983). The main goal of such algorithms is to track the ridges or valleys of the fringes in the intensity surface to create 1-pixel wide contours. Phase unwrapping techniques are used to order the contours in depth assuming adequate spacing between the contours. It is not possible to correctly interpolate the phase (depth) between the fringes because between-fringe gray level variations are a function of local contrast, local surface reflectance, and phase change due to distance.

5.2 Shadow Moire

If a surface is relatively flat, shadow moire can be used. A single grating of large extent is positioned near the object surface. The surface is illuminated through the grating and viewed from another direction. Everything is the same as projection moire except that two matched gratings are not needed. Cline et al. (1982, 1984) show experimental results where 512 × 512 range images of several different surfaces were obtained automatically using shadow moire methods.

5.3 Single frame moire with reference

The projected grating on a surface can be imaged directly by a camera without a camera grating, digitized, and "demodulated" via computer software provided that a reference image of a flat plane is also digitized. As a general rule of thumb, single frame systems of this type are able to resolve range proportional to about 1/20 of a fringe spacing. Idesawa et al. (1977, 1980) did early work in automated moire surface measurement.

Electro-Optical Information Systems, Inc. (1987) has a commercially available range-imaging sensor of this type. On appropriate surfaces, the system creates a 480 × 512 range image in about 2 s using two array processors and has 1 part in 4000 resolution (M = 350,540 assuming accuracy of 1 part in 1000).

5.4 Multiple-frame phase-shifted moire

Multiple-frame (N-frame) phase-shifted moire is similar to single-frame moire except that after the

first frame of image data is acquired, the projector grating is precisely shifted laterally in front of the projector by a small distance increment that corresponds to a phase shift of $360/N$ degrees and subsequent image frames are acquired. This method, similar to quasi-heterodyne holographic interferometry, allows for an order of magnitude increase in range accuracy compared to conventional methods. Halioua and Srinivasan (1987) present a detailed description of the general moire concept. Srinivasan et al. (1985) show experimental results for a mannequin head using $N = 3$. They obtained 0.1-mm range accuracy over a 100-mm depth of field ($M = 46{,}740$ assuming 2 min. computation time for 512×512 images). Other research in this area has been reported by Andersen (1986).

Boehnlein and Harding (1986) implemented this approach on special hardware. The computations take less than 3.5 s for a 256×256 image, but the high-accuracy phase-shifting translation device (accurate to 0.1 μ) limited them to about 10 s for complete range image acquisition. The range resolution of the system is 11 μ over a 64-mm depth of field ($M = 121{,}430$ assuming 1 part in 1500 accuracy).

6. Holographic Interferometry

Holography was introduced in 1961 by Leith and Upatnieks (1962). The principles of holographic interferometry were discovered soon after (see Vest 1979, Schuman and Dubas 1979). Holographic interferometers use coherent light from laser sources to produce interference patterns due to the optical-frequency phase differences in different optical paths. If two laser beams (same polarization) meet at a surface point $\mathbf{x}$, then the electric fields *add* to create the net electric field:

$$E(\mathbf{x}, t) = E_1 \cos(\omega_1 t - \mathbf{k}_1 \cdot \mathbf{x} + \phi_1(\mathbf{x})) + E_2 \cos(\omega_2 t - \mathbf{k}_2 \cdot \mathbf{x} + \phi_2(\mathbf{x})) \quad (12)$$

where the $\mathbf{k}_i$ are 3-D wave vectors pointing in the propagation directions with magnitude $\|\mathbf{k}_i\| = 2\pi/\lambda_i$, the $\omega_i = \|\mathbf{k}_i\|c$ are the radial optical frequencies, and $\phi_i(\mathbf{x})$ are the optical phases. Since photodetectors respond to the square of the electric field, the detectable irradiance (intensity) is $I(\mathbf{x}, t) = E^2(\mathbf{x}, t)$. Photodetectors themselves act as low-pass filters of the irradiance function I to yield the detectable interference signal $I'(\mathbf{x}, t) = \mathrm{LPF}[I(\mathbf{x}, t)]$, or

$$I'(\mathbf{x}, t) = E_a\{1 + E_b \cos[\Delta\omega t + \Delta\mathbf{k} \cdot \mathbf{x} + \Delta\phi(\mathbf{x})]\} \quad (13)$$

where

$$E_a = E_1^2 + E_2^2/2 \text{ and}$$
$$E_b = 2E_1E_2/(E_1^2 + E_2^2),$$

$\Delta\omega = \omega_1 - \omega_2$ is the difference frequency, $\Delta\mathbf{k} = \mathbf{k}_2 - \mathbf{k}_1$ is the difference wave vector, and $\Delta\phi(\mathbf{x}) = \phi_1 - \phi_2$ is the phase difference. This equation is of the exact same form as the moire equation (10) above for $A'(x)$ except that a time-varying term is included. Since phase changes are proportional to optical path differences in holographic interferometry, fraction of a wavelength distances can be measured. For equal optical frequencies and equal (wave vector) spatial frequencies, only the phase difference term remains. In holographic interferometric range sensors, surface depth information is encoded in and recovered from the phase difference term. Just as the z-depth spacing of moire fringes is proportional to the period of grating lines, the z-depth spacing of holographic interference fringes is proportional to the wavelength of the light. Measured object surfaces must be very flat and smooth.

6.1 Conventional Holography

Conventional interferometry is somewhat like conventional projection moire in that the frequencies of the interfering beams are equal and between-fringe ranging is not possible. There are three types of conventional holographic interferometry used in industrial applications: (1) real-time holography, which allows observers to see instantaneous microscopic changes in surface shape, (2) double-exposure holographic systems, which provide permanent records of surface shape changes, (3) time-average holography, which produces vibration mode maps useful for verifying finite element analyses.

Conventional holographic interferometry is used to visualize stress, thermal strains, pressure effects, erosion, microscopic cracks, fluid flow, and other physical effects in nondestructive testing. Tozer et al. (1985), Mader (1985), Wuerker and Hill (1985), and Church et al. (1985) provide a sampling of industrial uses of holographic interferometry. The Holomatic 8000 (Laser Technology 1986) and the HC1000 Instant Holographic Camera (10-s development time on erasable thermoplastic film) (Newport Corp. 1987) are commercially available holographic camera systems.

6.2 Heterodyne Holography

Heterodyne holographic interferometers cause two coherent beams of slightly different optical frequencies (less than 100 MHz generates RF beat frequencies) to interfere creating time-varying holographic

fringes in the image plane. Optical frequency shifts are achieved by acoustooptic modulators, rotating quarter wave plates, rotating gratings, and other methods. Optical phase measurements corresponding to optical path differences are made at each point by electronically measuring the phase of the beat frequency signal relative to a reference using a phasemeter. The time-varying interference fringe image is mechanically scanned with a high-speed detector to obtain a range image. Heterodyne holographic interferometers can make out-of-plane surface measurements with nanometer resolution over several microns, but they are typically slow. The general rule of thumb is that $\lambda/1000$ resolution is possible using heterodyne methods.

Pantzer et al. (1986) built a heterodyne profilometer that has a mechanical-vibration–limited range resolution of 5 nm and a lateral resolution of 3 μ. The theoretical resolution of this method is 0.4 nm if mechanical instabilities were removed. It took about 20 s to linearly scan 1 mm to get 330 points. (M = 2450 assuming a 3-μ depth of field).

Dandliker and Thalman (1985) obtained 0.2-nm range resolution over a depth of field of 3 μ at a rate of 1 point per second over a lateral range of 120 mm using a double-exposure heterodyne interferometer (M = 7500 assuming 0.4 nm accuracy).

Pryputniewicz (1985) used heterodyne interferometry to study the load-deformation characteristics of surface mount components on a printed circuit board. The reported 3σ range accuracy was 2 nm.

Sasaki and Okazaki (1986) developed a variation on frequency-shift heterodyne methods. The reference path mirror is mounted on a piezoelectric transducer (PZT) modulated at about 220 Hz. This phase modulation provides the needed small frequency shift for heterodyne accuracy. This is slow enough that image sensors can be used to collect the video signals. They obtained repeatable range measurements at less than 1 nm resolution. Over a 250 $\times$ 250 μ field of view, the lateral resolution is about 5 μ.

6.3 Quasi-Heterodyne (Phase-Shifted) Methods

Phase-shifted holographic interferometers are referred to as quasi-heterodyne since their $\lambda/100$ range resolution is not quite heterodyne performance, but is much better than conventional. Quasi-heterodyne systems can be much simpler, much cheaper, and much faster than heterodyne systems by trading off some range resolution. Standard video cameras can be used to image several frames of holographic fringes. Phase-shifts can be achieved at every pixel in parallel in real-time using a piezoelectric translator to move a mirror. (Compare this to the lateral shifting of a grating in front of a projector in phase-shifted moire.) Other phase-shifting methods are possible. The computations are very similar to those described in the previous section on multiple frame phase-shifted moire.

Hariharan (1985) used a 100 $\times$ 100 camera to digitize the holographic fringes needed to compute the range image. The measurement cycle for each fringe image was about 150 ms, and the total computation time was 10 s using a machine-language program. They used the same formulas as Boehnlein and Harding (1986) discussed above. Results are shown for a large 50 mm $\times$ 100 mm field of view (M = 8095 assuming 8-bit accuracy).

Thalman and Dandliker (1985) and Dandliker and Thalmann (1985) examine two-reference beam interferometry and two-wavelength contouring for quasi-heterodyne and heterodyne systems.

Chang et al. (1985) did experiments in digital phase-shifted holographic interferometry to eliminate the need to calibrate the phase shifter as in Hariharan et al. (1983). They claim an accuracy of 2 nm over a 300-nm depth of field.

6.4 Microscopic Interferometry

Peterson et al. (1984) measured VHS video tape surfaces with an interferometer obtaining 1 μ lateral resolution and 1 nm range repeatability.

Matthews et al. (1986) describe a phase-locked loop interferometric method where the two arms of a confocal interference microscope are maintained in quadrature by using an electrooptic phase modulator. Results are shown where the system scanned a 3-μ $\times$ 3-μ field of view over a depth of field of 300 nm in 2 s with a range accuracy of 1 nm (M = 27,150).

7. Focusing

Horn (1968), Tenenbaum (1970), Jarvis (1976), and Krotkov (1986) have discussed focusing for range determination. Figure 11 shows basic focusing relationships. Pentland (1987), Grossman (1987), Krotkov and Martin (1986), Schlag et al. (1983), Jarvis (1976), and Harvey et al. (1985) discuss passive methods to determine range from focus.

The autofocus mechanisms in cameras act as range sensors (Denstman 1980, Goldberg 1982), but most commercially available units do not use focusing principles to determine range. The Canon "Sure-Shot" autofocusing mechanism is an active triangulation system using a frequency modulated infrared beam. Jarvis (1982) used this Canon sensor

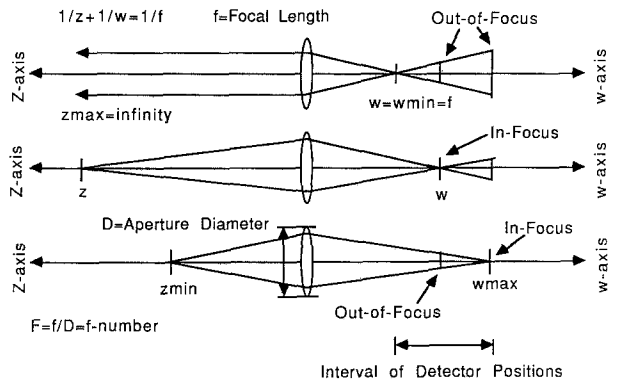

Figure 11: Thin lens relationships.

module to create a 64 × 64 range image in 50 min. The Honeywell Visitronic module for Konica, Minolta, and Yashica cameras is a passive triangulation system that correlates photocell readouts to achieve a binocular stereomatch and the corresponding distance. The Polaroid autofocusing mechanism is a broad beam sonar unit.

Rioux and Blais (1986) developed two techniques based on lens focusing properties. In the first technique, a grid of point sources is projected onto a scene. The range to each point is determined by the radius of the blur in the focal plane of the camera. The system was capable of measuring depths to 144 points with 1-mm resolution over a 100-mm depth of field. The second technique uses a multistripe illuminator. If a stripe is not in focus, the camera sees split lines where the splitting distance between the lines is related to the distance to the illuminated surface. Special purpose electronics process the video signal (Blais and Rioux 1986) and detect peaks to obtain line splitting distances on each scan line and hence range. The system creates a 256 × 240 range image in less than 1 s by analyzing 10 projected lines in each of 24 frames. The projected lines are shifted between each frame. A resolution of 1 mm over a depth of 250 mm is quoted at a 1-m standoff for a small robot-mountable unit (M = 63,450).

Kinoshita et al. (1986) developed a point range sensor based on a projected conical ring of light and focusing principles. A lens is mechanically focused to optimize the energy density at a photodiode. The prototype system measured range with a repeatability of 0.3 mm over a depth of field of 150 mm (9 bits) with a standoff distance of 430 mm.

Corle et al. (1987) measured distances with accuracies as small as 40 nm over a 4-μ depth of field using a type II confocal scanning optical microscope.

8. Fresnel Diffraction

Talbot (1836) first observed that if a line grating $T(x, y) = T(x + p, y)$ with period p is illuminated with coherent light, exact in-focus images of the grating are formed at regular periodic (Talbot) intervals D. This is the self-imaging property of a grating. Lord Rayleigh (1881) first deduced that $D = 2p^2/\lambda$ when $p \gg \lambda$. The Talbot effect has been analyzed more recently by Cowley and Moodie (1957) and Winthrop and Worthington (1965). For cosine gratings, grating images are also reproduced at $D/2$ intervals with a 180-deg phase shift. Thus, the ambiguity interval for such a range sensor is given by $I_r = p^2/2\lambda = D/4$. Ambiguity resolving techniques are needed for larger depths of field. The important fact is that the grating images are out of focus in a predictable manner in the ambiguity interval such that local contrast depends on the depth z. Figure 12 shows the basic configuration for measuring distance with the Talbot effect.

The Chavel and Strand (1984) method illuminates an object with laser light that has passed through a cosine grating. A camera views the object through a beam-splitter so that the grating image is superimposed on the returned object image that is modulated by (1) the distance to object surface points and by (2) the object surface reflectivity. The contrast ratio of the power in the fundamental frequency p^{-1} to the average (dc) power is proportional to depth and can be determined in real-time by analog video electronics. The analog range-image signal was digitized to create an 8-bit 512 × 512 image representing a 20 mm × 20 mm field of view approximately. The ambiguity interval was 38 mm. The digitizer averaged 16 frames so that the frame time is about 0.5 s (M = 92,680 assuming 7-bit accuracy).

Leger and Snyder (1984) developed two techniques for range imaging using the Talbot effect.

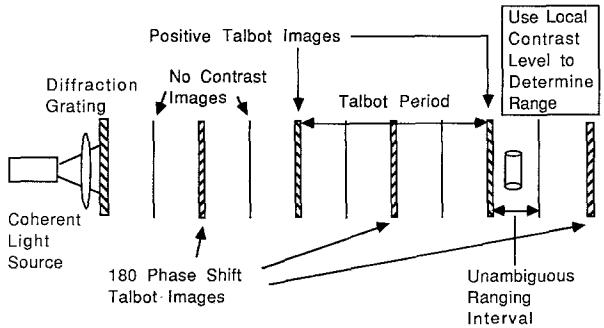

Figure 12. Talbot effect or self-imaging property of gratings for ranging.

The first method used two gratings crossed at right angles to provide two independent channels for depth measurement. The second method uses a modulated grating created by performing optical spatial filtering operations on the original signal emanating from a standard grating. Two prototype sensors were built to demonstrate these methods. The ambiguity intervals were 7.3 mm and 4.6 mm. The figure of merit is similar to the Chavel and Strand sensor. Speckle noise (Goodman 1986, Leader 1986) is a problem with coherent light in these methods, and good range resolution is difficult to obtain from local contrast measures. Other research in this area has been pursued by Hane and Grover (1985).

9. Sensor Comparisons

The key performance factors of any range-imaging sensor are listed in the following table:

Depth of field	L_r
Range accuracy	σ_r
Pixel dwell time	T
Pixel rate	$1/T$
Range resolution	N_{bits}
Image size	$N_x \times N_y$
Angular field of view	$\theta_x \times \theta_y$
Lateral resolution	$\theta_x/N_x \times \theta_y/N_y$
Standoff distance	L_s
Nominal field of view	$(L_s + L_r/2)\theta_x \times (L_s + L_r/2)\theta_y$
Frame time	$T \times N_x \times N_y$
Frame rate	$1/(T \times N_x \times N_y)$

The figure of merit M used to evaluate sensors in this survey only uses the first three values. A full evaluation for a given application should consider all sensor parameters.

Different types of range imaging sensors are compared by showing the rated sensors in the survey in two scatterplots. In Figure 13, range-imaging sensors are shown at the appropriate locations in a plot of (log) figure of merit M versus (log) range accuracy σ. In Figure 14, range imaging sensors are shown at the appropriate locations in a plot of (log) depth-of-field to range-accuracy ratio (number of accurate range bits) as a function of the (log) pixel dwell time. The two plots in Figures 13 and 14 display the quantitative comparisons of rated sensors and show the wide range of possible sensor performance.

9.1 General Method Comparisons

The six optical ranging principles are briefly summarized below. Imaging laser radars are capable of

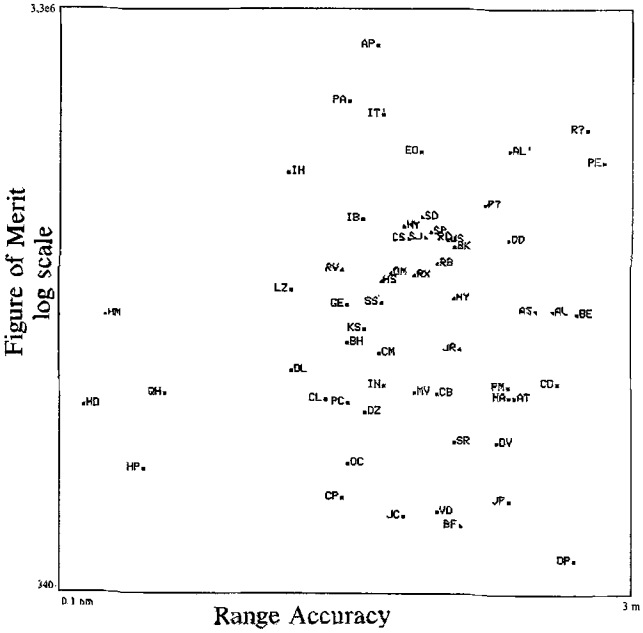

AL - Erim-ALV AL'- New-Erim-ALV AP - RVSI-APGMS
AS - Erim-ASV AT - ATT:Miller,Wagner BE - Boulder-ED
BF - Beheim-Fritsch BK - Bickel-et-al BK - Boyer-Kak-Color
CB - Cotter-Batch CD - Cathey,Davis CL - CyberOptics-LPS
CM - CMU:Kanade-Fuhrman CP - CyberOptics-PRS CS - Chavel-Strand
DL - Diffracto-LaserProbe DM - Hersman-DD-Metrol DV - Hersman-DD-Vision
DZ - Diffracto-Z-Series ED - EDIS:Fitts GE - GE:Mundy-Porter
HA - Heikkinen,Ahola HD - Dandliker-Thalmann HM - Matthews-et-al
HP - Pantzer-et-al HS - NYIT:Halioua-Srini HY - Hymarc-Hyscan
IB - ITI:Boehnlein-Harding IH - ITI:Harding-Goodson IN - Forstner-Indusurf
IT'- New-Erim-ITA JC - Jalkio-Kim-Case JP - JPL:Lewis-Johnston
JR - Jarvis-83 KS - Kern-SPACE LZ - Lorenz
MV - Mapvision-Haggren NY - NYU:Intensity-Ratio OC - Octek-Eyechrometer
OD - Odetics-Inc OP - Optech:Larsen500 P? - Perceptron-Radar
PA - Photonic-Automation PC - Perceptron-Contour PE - Perkin-Elmer
PM - Pipitone-Marshall QH - Hariharan R? - RVSI-Ross
RB - NRCC:Rioux-Blais RC - RCA:Rosenfeld-Tsiks RV - RVSI-other
RX - NRCC:Rioux SJ - ServoRobot-Jupiter SO - Selcom-Optocator
SP - Solid-Photography SR - SRI:Nitzan,et-al SS - ServoRobot-Saturn
VO - Vuylsteke,Oosterlinck WS - Tech-Arts-White

Figure 13. Figure of merit vs. range accuracy.

range accuracies from about 50 μ to 5 m over depths of field 250 to 25,000 times larger. They benefit from having very small source to detector separations and operate at higher speeds than many other types of range-imaging sensors because range is determined electronically. They are usually quite expensive, with commercially available units starting at around $100,000. Existing laser radars are sequential in data acquisition (they acquire one point at a time) although parallel designs have been suggested.

Triangulation sensors are capable of range accuracies beginning at about 1 μ over depths of field from 250 to 60,000 times larger. In the past, some have considered triangulation systems to be inaccurate or slow. Many believe that large baselines are required for reasonable accuracy. However, triangulation systems have shown themselves to be accurate, fast, and compact mainly owing to the advent of synchronous scanning approaches. Simple triangulation systems start between $1000 and

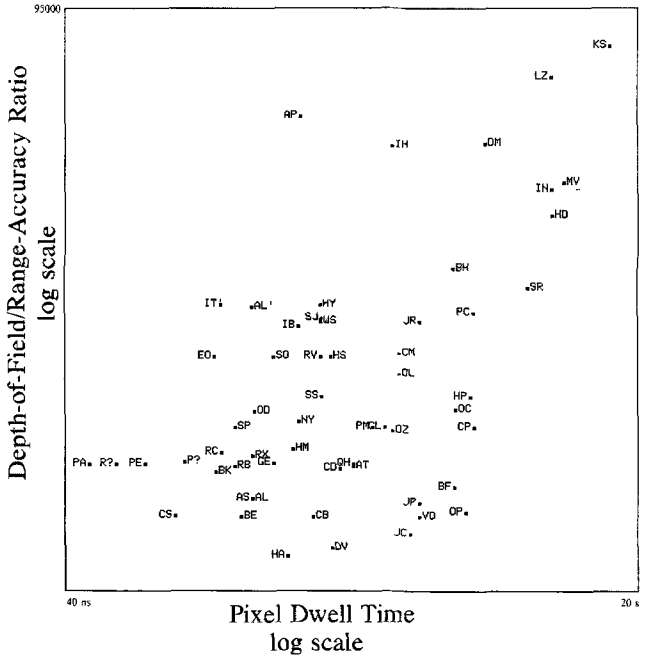

AL - Erim-ALV
AL'- New-Erim-ALV
AP - RVSI-APOMS
AS - Erim-ASV
AT - ATT:Miller,Wagner
BE - Boulder-EO
BF - Beheim-Fritsch
BH - Bickel-et-al
BK - Boyer-Kak-Color
CB - Cotter-Batch
CD - Cathey,Davis
CL - CyberOptics-LRS
CM - CMU:Kanade-Fuhrman
CP - CyberOptics-PRS
CS - Chavel-Strand
DL - Diffracto-LaserProbe
DM - Hersman-DO-Metrol
DV - Hersman-DO-Vision
DZ - Diffracto-Z-Series
EO - EOIS:Fitts
GE - GE:Mundy-Porter
HA - Heikkinen,Ahola
HD - Dandliker-Thalmann
HM - Matthews-et-al
HP - Pantzer-et-al
HS - NYIT:Halioua-Srini
HY - Hymarc-Hyscan
IB - ITI:Boehnlein-Harding
IH - ITI:Harding-Goodson
IN - Forstner-Indusurf
IT'- New-Erim-ITA
JC - Jalkio-Kim-Case
JP - JPL:Lewis-Johnston
JR - Jarvis-83
KS - Kern-SPACE
LZ - Lorenz
MV - Mapvision-Haggren
NY - NYU:Intensity-Ratio
OC - Octek-Eyechrometer
OD - Odetics-Inc
OP - Optech:Larsen500
P? - Perceptron-Radar
PA - Photonic-Automation
PC - Perceptron-Contour
PE - Perkin-Elmer
PM - Pipitone-Marshall
QH - Hariharan
R? - RVSI-Ross
RB - NRCC:Rioux-Blais
RC - RCA:Rosenfeld-Tsiks
RV - RVSI-other
RX - NRCC:Rioux
SJ - ServoRobot-Jupiter
SO - Selcom-Optocator
SP - Solid-Photography
SR - SRI:Nitzan,et-al
SS - ServoRobot-Saturn
VC - Vuylsteke,Oosterlinck
WS - Tech-Arts-White

Figure 14. Depth-of-field/range-accuracy ratio versus pixel dwell time.

$10,000 depending on how much you put together yourself and how much needed equipment you already have. Commercially available turnkey systems can easily run upwards of $50,000, and fancier systems can run into the hundreds of thousands if there are requirements for fine accuracy over large working volumes. Triangulation systems go from totally sequential as in point scanners to almost parallel as in the intensity ratio scheme or the color encoded stripe scheme. Triangulation systems have been the mainstay of range imaging and promise to remain so.

Moire systems are limited to about the same accuracies as triangulation sensors (a few microns) and are not applicable unless surface slope constraints are satisfied. The depth of field of a moire system depends on the camera resolution and the object grating period p_o. For a 512 × 512 camera and a minimum of about 5 pixels per fringe, 100 phase transitions can be unwrapped yielding a depth of field on the order of 100 p_o. Optical moire components are a small part of the total system cost if fast computer hardware is used to carry out the necessary computations. Image array processors vary in cost, but a complete moire system with reasonable speed will probably run more than $50,000. Moire techniques are inherently parallel and will benefit from the development of parallel computing hardware.

Holographic interferometer systems can measure with accuracies of less than half a nanometer over as many wavelengths of light as can be disambiguated. Surface slope and smoothness constraints must be met before holographic methods are valid. The most accurate heterodyne methods are also the slowest and the most expensive. The quasi-heterodyne methods are faster and cheaper, but give up about an order of magnitude in accuracy compared to heterodyne. Holographic techniques are also inherently parallel and should benefit from the development of parallel computing hardware. Holographic systems are generally much more specialized than other optical techniques, and are applicable to fine grain surface inspection and nondestructive testing.

The Fresnel diffraction techniques based on the Talbot effect offer video frame rate range images using special-purpose analog video electronics. The range resolution of these systems is limited by the resolution of local contrast measures; it appears to be difficult to get more than seven or eight bits of range. Diffraction ranging is also inherently parallel.

Active focusing methods have great potential for compact, inexpensive range-imaging sensors, but high-precision systems are not likely.

Tactile methods still dominate many potential range-imaging applications where industry needs to exactly specify the shape of a prototype object. The reliability and accuracy of coordinate measuring machines (CMM's) over very large working volumes are hard to beat, but they are inherently slow and very expensive. If flexible noncontact optical methods can provide similar performance with reliability and ease of use, then a significant cost savings will be realized in applications currently requiring CMM's. At very fine scales, the (nonoptical) scanning tunneling microscope (Binnig and Rohrer 1985) is the state-of-the-art in very accurate (0.01 nm) surface studies. It is clear that active, optical ranging sensors have competition from other techniques.

Comments from this section and the survey are summarized in Figure 15. The first range value for each method in this table (ACC) is a good nominal accuracy rounded to the nearest power of ten

Category	ACC/DOF	Notes
Radar (Pulse,AM,FM)	0.1 mm 100 m	Detect Time, Phase, or Frequency Differences Signal Depends on Range, Surface Normal, Reflectance Beam Scanning Usually Required, No Computation History: Since 1903, Well known since 40's, Lasers since 70's Cost: Inexpensive to Extremely Expensive
Triangulation	1 μm 100 m	1 or More Cameras, 1 or more Projectors Scanned Point, Scanned Stripe, Multi-Stripe, Grid Binary Pattern, Color, Texture, Intensity Ratio Terms: Synchronous Scan, Scheimpflug Condition History: Since 200 B.C., Most Popular Method Cost: Inexpensive to Very Expensive
Moire Techniques	1 μm 10 m	Projector, Grating(s), Camera, Computer Fringe Tracking: Projection, Shadow Reference: Single-Frame, Multi-Frame (Phase-Shifted) Surface Slope Constraint, Non-coherent Light Computation Required, No Scanning History: Since 1859, Used Since 1950's in Mech.Eng. Cost: Inexpensive (excluding Computer)
Holographic Interferometry	0.1 nm 100 μm	Detector, Laser, Optics, Electronics, Computer Conventional: Real-Time, 2-Exposure, Time-Avg. Quasi-Heterodyne (Phase-Shifted), Heterodyne Surface Slope Constraint, Coherent Light Computation/Electronics Required, No Scanning History: Not Practical until Laser 1961, Big in NDT Cost: Inexpensive to Expensive
Focusing	1 mm 10 m	Measure Local Contrast, Blur, Displacement Limited Depth-of-Field to Accuracy Ratio History: Since 1800's, Gauss thin lens law Computation/Electronics Required, No Scanning Potential for Inexpensive Systems
Fresnel Diffraction (Talbot Effect)	0.1 mm 10 m	Laser, Grating, Camera / Not Explored by Many Video Rates, Limited Accuracy, Uses Local Contrast Electronics Required, No Scanning History: Discovered 1836, Used 1983 Potential for Inexpensive Systems

Figure 15. General comments on fundamental categories.

whereas the second value is the maximum nominal depth of field. Figure 16 indicates in a brief format the types of applications where the different ranging methods are being used or might be used.

10. Emerging Themes

As in any field, people always want equipment to be faster, more accurate, more reliable, easier to use, and less expensive. Range-imaging sensors are no exception. But compared to the state of the art 10 years ago, range imaging has come a long way. An image that took hours to acquire now takes less than a second. However, the sensors are only one part of the technology needed for practical automated systems. Algorithms and software play an even bigger role, and although research in range-image analysis and object recognition using range images (Besl and Jain 1985) has come a long way in recent years, there is still much to be done to achieve desired levels of performance for many applications.

Application	Radar	Trian	Moire	Holog	Focus	Diffr
Cartography	X	X				
Navigation	X	X			X	
Medical	X	X	X			
Shape Definition	X	X	X	X		
Bin Picking	X	X			X	X
Assembly	X	X	X	X	X	X
Inspection	X	X	X	X		X
Gauging	X	X	X	X		X

Figure 16. Methods and applications of range-imaging sensors.

Image acquisition speed is a critical issue. Since photons are quantized, the speed of data acquisition is limited by the number of photons that can be gathered by a pixel's effective photon collecting area during the pixel dwell time. Greater accuracy or faster frame times are possible using higher energy lasers since more photons can be collected reducing shot noise and improving signal-to-noise ratio. But today's higher-power laser diodes are difficult to focus to a small point size because of irregularities in the beam shapes. Moreover, higher-power lasers are a greater threat to eye safety if people will be working close to the range-imaging sensors (see appendix). Longer wavelengths (1.3–1.55 μ) are desirable for better eye safety, but not enough power is available from today's laser diodes at these wavelengths to obtain reasonable quality range images. The fiber optics communications industry is driving the development of longer wavelength laser diodes, and hopefully this situation will soon be remedied.

Another issue in the speed of data acquisition is scanning mechanisms. Many sensors are limited by the time for a moving part to move from point A to point B. Image dissector cameras are being explored by several investigators to avoid mechanical scanning. Mechanical scanning is a calibration and a reliability problem because moving parts do eventually wear out or break. However, today's mechanical scanners can offer years of reliable service.

Once considered state-of-the-art, 8-bit resolution sensors are giving way to sensors with 10 to 12 bits or more of resolution and possibly accuracy. Processing this information with inexpensive image processing hardware designed for 8-bit images is inappropriate. A few commercial vendors provide 16-bit and floating point image processing hardware, but it is generally more expensive.

Reliable subpixel image location is being achieved in many single light stripe triangulation sensors. It is commonly accepted that a fourth, a fifth, an eighth, or a tenth of a pixel accuracy can realistically be obtained with intensity weighted averaging techniques. Moreover, Kalman filtering (recursive least squares) algorithms (see e.g. Smith and Cheeseman 1987) are beginning to be used in vision algorithms for optimally combining geometric information from different sensing viewpoints or different range sensors. Such efforts will continue to increase the accuracy of sensors and systems.

Although not specifically mentioned, many range sensors also acquire registered intensity images at the same time. Although there is little 3-D metrology information in these images, there is a great

deal of other useful information that is important for automated systems. A few researchers have addressed methods for using this additional information, but commercially available software solutions are more than several years away.

Range-imaging sensors are the data-gathering components of range-imaging systems, and ranging imaging systems are machine perception components of application systems. Algorithms, software, and hardware are typically developed in isolation and brought together later, but there are trends toward developing hardware that can incorporate programmability features that expedite operations common to many applications.

Acknowledgments. The author would like to express his appreciation to R. Tilove and W. Reguiro for their thorough reviews, and to G. Dodd, S. Walter, R. Khetan, J. Szczesniak, M. Stevens, S. Marin, R. Hickling, W. Wiitanen, R. Smith, T. Sanderson, M. Dell'Eva, H. Stern, and J. Sanz.

References

Agin GJ, Highnam, PT (1983) Movable light stripe sensor for obtaining 3D coordinate measurements. Proceedings SPIE Conference on 3-D Machine Perception (360):326

Ahola R, Heikkinen T, Manninen M (1985) 3D image acquisition by scanning time of flight measurements. Proceedings International Conference on Advances in Image Processing and Pattern Recognition

Altschuler MD, Altschuler BR, Toboada J (1981) Laser electro-optic system for rapid 3D topographic mapping of surfaces. Optical Engineering 20(6):953–961

Andresen K (1986) The phase shift method applied to moire image processing. Optik 72:115–119

ANSI 1986. American National Standard for the safe use of lasers. (ANSI Z136.1-1986) American National Standards Institute, New York

Asada M, Ichikawa H, Tsuji S (1986) Determining surface property by projecting a stripe pattern. Proceedings International Conference on Pattern Recognition IEEE-CS, IAPR: 1162–1164

Banic J, Sizgoric S, O'Neill R (1987) Airborne scanning lidar bathymeter measures water depth. Laser Focus/ Electro-Optics: 48–52

Bastuschek CM, Schwartz JT (1984) Preliminary implementation of a ratio image depth sensor. Robotics Research Report No. 28, Courant Institute of Mathematical Sciences, New York University, New York

Beheim G, Fritsch K (1986) Range finding using frequency-modulated laser diode. Applied Optics, 25(9):1439–1442

Besl PJ (1987) Range imaging sensors. Tech. Report GMR-6090. Computer Science Dept., General Motors Research Labs, Warren, MI

Besl PJ (1988) Active optical range imaging sensors. In: Advances in Machine Vision: Architectures and Applications. J. Sanz (Ed.), Springer-Verlag, New York

Besl PJ, Jain RC (1985) Three dimensional object recognition. ACM Computing Surveys 17(1):75–145

Bickel G, Hausler G, Maul M (1984) Optics in Modern Science and Technology, Conf. Dig. ICO-13:534

Bickel G, Hausler G, Maul M (1985) Triangulation with expanded range of depth. Optical Engineering 24(6):975–979

Binger N, Harris SJ (1987) Applications of laser radar technology. Sensors 4(4):42–44

Binnig G, Rohrer H (1985) The scanning tunneling microscope. Scientific American 253,2 (Aug), 50–69

Blais F, Rioux M (1986) Biris: a simple 3D sensor. Proceedings SPIE Conference on Optics, Illumination, and Image Sensing for Machine Vision, 728:235–242

Boehnlein AJ, Harding KG (1986) Adaptation of a parallel architecture computer to phase-shifted moire interferometry. Proceedings SPIE Conference on Optics, Illumination, and Image Sensing for Machine Vision, 728:132–146

Boulder Electro-Optics (1986) Product information, Boulder, Colorado. (now Boulder Melles Griot)

Boyer KL, Kak AC (1987) Color encoded structured light for rapid active ranging. IEEE Transactions Pattern Analysis Machine Intelligence PAMI-9, 1:14–28

Brou P (1984) Finding the orientation of objects in vector maps. International Journal of Robot Research 3:4

Bumbaca F, Blais F, Rioux M (1986) Real-time correction of 3D nonlinearities for a laser rangefinder. Optical Engineering 25(4):561–565

Carrihill B (1986) The intensity ratio depth sensor. Ph.D. dissertation, Courant Institute of Mathematical Sciences, New York University, New York

Carrihill B, Hummel R (1985) Experiments with the intensity ratio depth sensor. Computer Vision, Graphics, Image Processing 32:337–358

Case SK, Jalkio JA, Kim RC (1987) 3D vision system analysis and design. In: Three-Dimensional Machine Vision, T. Kanade (Ed.), Kluwer Academic, Boston, pp. 63–96

Cathey WT, Davis WC (1986) Vision system with ranging for maneuvering in space. Optical Engineering 24(7):821–824. See also Imaging system with range to each pixel. Journal of the Optical Society of America A 3(9):1537–1542

CDRH 1985. Federal Register, Part III, Dept. of Health and Human Services, 21 CFR Parts 1000 and 1040 [Docket No. 80N-0364], Laser Products; Amendments to Performance Standard; Final Rule. For further info, Contact Glenn Conklin, Center for Devices and Radiological Health (HFZ-84), U.S. Food and Drug Administration, 5600 Fishers Lane, Rockville, MD 20857

Chang M, Hu CP, Lam P, Wyant JC (1985) High precision deformation measurement by digital phase shifting holographic interferometry. Applied Optics 24(22):3780–3783

Chavel P, Strand TC (1984) Range measurement using Talbot diffraction imaging of gratings. Applied Optics 23(6):862–871

Church EL, Vorburger TV, Wyant JC (1985) Direct comparison of mechanical and optical measurements of the finish of precision machined optical surfaces. Optical Engineering 24(3):388–395

Cline HE, Holik AS, Lorenson WE (1982) Computer-aided surface reconstruction of interference contours. Applied Optics 21(24):4481–4489

Cline HE, Lorenson WE, Holik AS (1984) Automated moire contouring. Applied Optics 23(10):1454–1459

Corle TR, Fanton JT, Kino GS (1987) Distance measurements by differential confocal optical ranging. Applied Optics 26(12):2416–2420

Cotter SM, Batchelor BG (1986) Deriving range maps at real-time video rates. Sensor Review 6(4):185–192

Cowley JM, Moodie AF (1957) Fourier images: I—the point source. Proceedings Physical Society 70:486–496

Cunningham R (1986) Laser radar for the space conscious. Lasers and Applications July: 18–20

Cyberoptics (1987) Product information. Minneapolis, MN

Damm L (1987) A minimum-size all purpose fiber optical proximity sensor. Proceedings Vision'87 Conference: 6-71—6-91

Dandliker R, Ineichen B, Mottier F (1973) Optics Communications 9:412

Dandliker R (1980) Heterodyne holography review. Progress in Optics 17:1

Dandliker R, Thalmann R (1985) Heterodyne and quasi-heterodyne holographic interferometry. Optical Engineering 24(5):824–831

Dandridge A (1982) Current induced frequency modulation in diode lasers. Electron. Letters 18:302

Denstman H (1980) State-of-the-art optics: Automated image focusing. Industrial Photography, July: 33—37

Dereniak EL, Crowe DG (1984) Optical Radiation Detectors. Wiley, New York

Diffracto (1987) Product Literature. Laser probe digital ranging sensor. Diffracto, Ltd., Windsor, Canada

Digital Optronics (1986) Product literature. Springfield, VA

Dimatteo PL, Ross JA, Stern HK (1979) Arrangement for sensing the geometric characteristics of an object. (RVSI) U.S. Patent 4175862

Electro-Optical Information Systems (1987) Product Information. EOIS, Santa Monica, CA

Faugeras OD, Hebert M (1986) The representation, recognition, and locating of 3-D objects. International Journal of Robotic Research 5(3):27–52

Froome KD, Bradsell RH (1961) Distance measurement by means of a light ray modulated at a microwave frequency. Journal of Scientific Instrumentation 38:458–462

Gasvik KJ (1983) Moire technique by means of digital image processing. Applied Optics 22(23):3543–3548

Goldberg N (1982) Inside autofocus: How the magic works. Popular Photography, Feb: 77–83

Goodman JW (1986) A random walk through the field of speckle. Optical Engineering 25(5):610–612

Gottlieb M (1983) Electro-Optic and Acousto-Optic Scanning and Deflection. Marcel-Dekker, New York

Griffin DR (1958) Listening in the dark: The acoustic orientation of bats and men. Yale University Press, New Haven, CT

Grossman P (1987) Depth from Focus. Pattern Recognition Letters 5(1):63–69

Haggren H, Leikas E (1987) Mapvision—The photogrammetric machine vision system. Proceedings Vision'87 Conference: 10-37–10-50

Halioua M, Srinivasan V (1987) Method and apparatus for surface profilometry. New York Institute of Technology, Old Westury, NY. U.S. Patent 4,641,972

Halioua M, Krishnamurthy RS, Liu H, Chiang FP (1983) Projection moire with moving gratings for automated 3D topography. Applied Optics 22(6):850–855

Hall EL, Tio JBK, McPherson CA, Sadjadi FA (1982) Measuring curved surfaces for robot vision. Computer 15(12):42–54

Hane K, Grover CP (1985) Grating imaging and its application to displacement sensing. Journal of Optical Society of America A 2(13):9

Harding KG (1983) Moire interferometry for industrial inspection. Lasers and Applications Nov.: 73

Harding KG, Goodson K (1986) Hybrid high accuracy structured light profiler. Proceedings SPIE Conference on Optics, Illumination, and Image Sensing for Machine Vision 728:132–145

Harding KG, Tait R (1986) Moire techniques applied to automated inspection of machined parts. Proceedings Vision'86 Conference, SME, Dearborn, MI

Hariharan P (1985) Quasi-heterodyne hologram interferometry. Optical Engineering 24(4):632–638

Hariharan P, Oreb BF, Brown N (1983) Applied Optics 22(6):876

Harvey JE, MacFarlane MJ, Forgham JL (1985) Design and performance of ranging telescopes: Monolithic vs. synthetic aperture. Optical Engineering 24(1):183–188

Hausler G, Maul M (1985) Telecentric scanner for 3D sensing. Optical Engineering 24(6):978–980

Heikkinen T, Ahola R, Manninen M, Myllyla R (1986) Recent results of the performance analysis of a 3D sensor based on time of flight. Proceedings SPIE Quebec International Symposium on Optical and Optoelectronic Applied Sciences and Engineering.

Hersman M, Goodwin F, Kenyon S, Slotwinski A (1987) Coherent laser radar application to 3D vision and metrology. Proceedings Vision'87 Conference 3-1–3-12

Holland SW, Rossol L, Ward MR (1979) Consight-1: A vision controlled robot system for transferring parts from belt conveyors. In: Computer Vision and Sensor-Based Robots G.G. Dodd and L. Rossol (Eds.), Plenum Press, New York, pp. 81–97

Horn BKP (1968) Focusing. MIT, Project MAC, AI Memo 160

Hulsmeyer C (1904) Hertzian wave projecting and receiving apparatus adapted to indicate or give warning of the presence of a metallic body, such as a ship or a train, in the line of projection of such waves. U.K. Patent 13,170

HYMARC (1987) Product information. Ottawa, Ontario Canada

Idesawa M, Yatagai Y, Soma T (1976) A method for the automatic measurement of 3D shapes by new type of moire topography. Proceedings 3rd International Conference Pattern Recognition: 708

Idesawa M, Yatagai Y, Soma T (1977) Scanning moire method and automatic measurement of 3D shapes. Applied Optics 16(8):2152–2162

Idesawa M, Yatagai Y (1980) 3D shape input and processing by moire technique. Proceedings 5th International Conference Pattern Recognition, IEEE-CS: 1085–1090

Idesawa M, Kinoshita G (1986) New type of miniaturized optical range sensing methods RORS and RORST. Journal of Robotic Systems 3(2):165–181

Inokuchi S, Sato K, Matsuda F (1984) Range imaging system for 3-D object recognition. Proceedings 7th International Conference Pattern Recognition: 806–808

Jalkio J, Kim R, Case S (1985) 3D inspection using multistripe structured light. Optical Engineering 24(6):966–974

Jalkio J, Kim R, Case S (1986) Triangulation based range sensor design. Proceedings SPIE Conference on Optics, Illumination, and Image Sensing for Machine Vision, 728:132–146

Jarvis RA (1976) Focus optimization criteria for computer image processing. Microscope 24(2):163–180

Jarvis RA (1982) Computer vision and robotics laboratory. IEEE Computer 15(6):9–23

Jarvis RA (1983a) A laser time-of-flight range scanner for robotic vision. IEEE Transactions Pattern Analysis Machine Intelligence PAMI-5, 5:505–512

Jarvis RA (1983b) A perspective on range finding techniques for computer vision. IEEE Transactions Pattern Analysis Machine Intelligence PAMI-5, 2:122–139

Jelalian AV, McManus RG (1977) AGARD Panel Proceeding No. 77. June, Sec. 2.1, pp 1–21

Johnson M (1985) Fiber displacement sensors for metrology and control. Optical Engineering 24(6):961–965

Kak AC (1985) Depth perception for robot vision. In: Handbook of Industrial Robotics, S. Nof (Ed.) Wiley, New York, pp 272–319

Kanade T, Asada H (1981) Noncontact visual 3D range-finding devices. In: Proceedings SPIE 3D Machine Perception, B.R. Altschuler (Ed.):48–53

Kanade T, Fuhrman M (1985) A noncontact optical proximity sensor for measuring surface shape. In: Three-Dimensional Machine Vision, T. Kanade (Ed.), Kluwer Academic Boston, pp 151–194

Karara HM (1985) Close-range photogrammetry: where are we and where are we heading? Photogrammetric Engineering and Remote Sensing 51(5):537–544

Kawata H, Endo H, Eto Y (1985) A study of laser radar. Proceedings 10th International Technical Conference on Experimental Safety Vehicles

Kellogg WN (1961) Porpoises and sonar. University of Chicago Press, Chicago, IL

Kern Instruments (1987) Product Information. Gottwald, R. and Berner, W., The new Kern system for positioning and automated coordinate evaluation; advanced technology for automated 3D coordinate determination. Brewster, NY. and Aarau, Switzerland

Keyes RJ (1986) Heterodyne and nonheterodyne laser transceivers. Review of Scientific Instrumentation 57(4):519–528

Khetan RP (1975) The theory and application of projection moire methods. Ph.D. dissertation. Dept. of Engineering Mechanics, State University of New York, Stony Brook

Kingslake R (1983) Optical system design, Academic Press, New York

Kinoshita G, Idesawa M, Naomi S (1986) Robotic range sensor with projection of bright ring pattern. Journal of Robotic Systems 3(3):249–257

Koenderink JJ, Van Doorn AJ (1986) Dynamic shape. Biological Cybernetics 53:383–396

Kratky V (1979) Real-time photogrammetric support of dynamic 3D control. Photogrammetric Engineering and Remote Sensing 45(9):1231–1242

Krotkov EP (1986) Focusing. Ph.D. Dissertation, U. Penn, Phila, PA

Krotkov E, Martin JP (1986) Range from focus. Proceedings IEEE International Conference on Robotics and Automation, IEEE-CS: 1093–1098

Kurahashi A, Adachi M, Idesawa M (1986) A prototype of optical proximity sensor based on RORS. Journal of Robotic Systems 3(2):183–190

Labuz J, McVey ES (1986) Camera and projector motion for range mapping. Proceedings SPIE Conference on Optics, Illumination, and Image Sensing for Machine Vision 728:227–234

Lamy F, Liegeois C, Meyrueis P (1981) 3D automated pattern recognition using moire techniques. Proceedings SPIE 360:345–351

Landman MM, Robertson SJ (1986) A flexible industrial system for automated 3D inspection. Proceedings SPIE Conference on Optics, Illumination, and Image Sensing for Machine Vision, 728:203–209

Laser Technology (1986) Product information. Norristown, PA

Leader JC (1986) Speckle effects on coherent laser radar detection efficiency. Optical Engineering 25(5):644–650

Leger JR, Snyder MA (1984) Real-time depth measurement and display using Fresnel diffraction and white-light processing. Applied Optics 23(10):1655–1670

Leith E, Upatnieks J (1962) Reconstructed wavefronts and communication theory. Journal of Optical Society America 54:1123–1130

Lewis RA, Johnston AR (1977) A scanning laser rangefinder for a robotic vehicle. Proceedings 5th International Joint Conference on Artificial Intelligence: 762–768

Lewis JRT, Sopwith T (1986) 3D surface measurement by microcomputer. Image and Vision Computing 4(3):159–166

Livingstone FR, Tulai AF, Thomas MR (1987) Application of 3-D vision to the measurement of marine propellers. Proceedings Vision'87 Conference: 10-25–10-36

Livingstone FR, Rioux M (1986) Development of a large field of view 3D vision system. Proceedings SPIE 665

Lord Rayleigh (JW Strutt) (1874) On the manufacture and theory of diffraction gratings. Phil. Mag. 47(81):193

Lord Rayleigh (JW Strutt) (1881) Phil. Mag. 11:196

Lorenz RD (1984) Theory and design of optical/electronic probes for high performance measurement of parts. Ph.D. dissertation, Univ. of Wisconsin-Madison

Lorenz RD (1986) A novel, high-range-to-resolution ratio, optical sensing technique for high speed surface geometry measurements. Proceedings SPIE Conference on Optics, Illumination, and Image Sensing for Machine Vision 728:152–146

Macy WW (1983) Two-dimensional fringe pattern analysis. Applied Optics 22(22):3893–3901

Mader DL (1985) Holographic interferometry of pipes: precision interpretation by least squares fitting. Applied Optics 24(22):3784–3790

Marshall G (1985) Laser Beam Scanning, Marcel-Dekker, New York

Matsuda R (1986) Multifunctional optical proximity sensor using phase modulation. Journal of Robotic Systems 3(2):137–147

Matthews HJ, Hamilton DK, Sheppard CJR (1986) Surface profiling by phase-locked interferometry. Applied Optics 25(14):2372–2374

Mersch SH, Doles JE (1985) Cylindrical optics applied to machine vision. Proceedings Vision'85 Conference, SME, 4-53–4-63

Mertz L (1983) Real-time fringe pattern analysis. Applied Optics 22(10):1535–1539

Miller GL, Wagner ER (1987) An optical rangefinder for autonomous robot cart navigation. Proceedings SPIE Industrial Electronics, Cambridge, MA, (November)

Moore DT, Traux BE (1979) Phase-locked moire fringe analysis for automated contouring of diffuse surfaces. Applied Optics 18(1):91–96

Mundy JL, Porter GB (1986) A three-dimensional sensor based on structured light. In: Three-Dimensional Machine Vision, T. Kanade (Ed.), Kluwer Academic, Boston, pp 3–62

Nakagawa Y, Ninomiya T (1987) Three-dimensional vision systems using the structured light method for inspecting solder joints and assembly robots. Three-Dimensional Machine Vision, T. Kanade (Ed.), Kluwer Academic, Boston, pp 543–565

Nevatia R, Binford TO (1973) Structured descriptions of complex objects. Proceedings 3rd International Joint Conference on Artificial Intelligence: 641–647

Newport Corp (1987) Product Information. Design and testing with holography. Machine vision components. Fountain Valley, CA

Nitzan D, Brain AE, Duda RO (1977) The measurement and use of registered reflectance and range data in scene analysis. Proceedings IEEE 65(2):206–220.

Nitzan D, Bolles R, Kremers J, Mulgaonkar P (May 1986) 3D vision for robot applications. NATO Workshop on Knowledge Engineering for Robotic Applications, Maratea, Italy

Oboshi T (1976) Three-Dimensional Imaging Techniques. Academic Press, New York

Oster G (1965) Moire optics: a bibliography. Journal of Optical Society America 55:1329

Ozeki O, Nakano T, Yamamoto S (1986) Real-time range measurement device for 3D object recognition. IEEE Trans. Pattern Analysis Machine Intelligence. PAMI-8, 4, 550–553

Pantzer D, Politch J, Ek L (1986) Heterodyne profiling instrument for the angstrom region. Applied Optics 25(22):4168–4172

Parthasarathy S, Birk J, Dessimoz J (1982) Laser rangefinder for robot control and inspection. Proceedings SPIE Robot Vision 336:2–11

Pelowski KR (1986) 3D measurement with machine vision. Proceedings Vision'86 Conference: 2-17–2-31

Pentland AP (1987) A new sense of depth of field. IEEE Transaction Pattern Analysis Machine Intelligence PAMI-9, 4:523–531

Perceptron (1987) Product information. Farmington Hills, MI

Perrin JC, Thomas A (1979) Electronic processing of moire fringes: application to moire topography and comparison with photogrammetry. Applied Optics 18(4):563–574

Peterson RW, Robinson GM, Carlsen RA, Englund CD, Moran PJ, Wirth WM (1984) Interferometric measurements of the surface profile of moving samples. Applied Optics 23(10):1464–1466

Photonic Automation, Inc. (1987) Product literature. Improving automated SMT inspection with 3D vision. M. Juha and J. Donahue. Santa Ana, CA

Pipitone FJ, Marshall TG (1983) A wide-field scanning triangulation rangefinder for machine vision. International Journal of Robotics Research 2(1):39–49

Pinckney HFL (1978) Theory and development of an online 30 Hz video photogrammetry system for real-time 3D control. International Archives of Photogrammetry, Vol. XXII, Part V. 2:38 pages

Pirodda L (1982) Shadow and projection moire techniques for absolute and relative mapping of surface shapes. Optical Engineering 21:640

Popplestone RJ, Brown CM, Ambler AP, Crawford GF (1975) Forming models of plane-and-cylinder faceted bodies from light stripes. Proceedings 4th International Joint Conference on Artificial Intelligence: 664–668

Potmesil M (1983) Generating models of solid objects by matching 3D surface segments. Proceedings 8th International Joint Conference on Artificial Intelligence: 1089–1093

Potsdamer J, Altschuler M (1982) Surface measurement by space-encoded projected beam system. Computer Graphics Image Processing 18:1–17

Pryputniewicz RJ (1985) Heterodyne holography applications in studies of small components. Optical Engineering 24(5):849–854

Quist TM, Bicknell WE, Bates DA (1978) ARPA Semiannual report: optics research, Lincoln Laboratory, MIT

Reid GT (1986) Automatic fringe pattern analysis: A review. Optics and Lasers in Engineering 7:37–68

Rioux M (1984) Laser range finder based upon synchronized scanners. Applied Optics 23(21):3837–3844

Rioux M, Blais F (1986) Compact 3-D camera for robotic applications. Journal of Optical Society of America A 3(9):1518–1521

Robotic Vision Systems, Inc (1987) Product literature. RVSI, Hauppage, NY

Rocker F (1974) Localization and classification of 3D objects. Proceedings 2nd International Conference Pattern Recognition: 527–528

Rosenfeld JP, Tsikos CJ (1986) High-speed space encoding projector for 3D imaging. Proceedings SPIE Conference on Optics, Illumination, and Image Sensing for Machine Vision, 728:146–151

Ross JA (1978) Methods and systems for 3D measurement. U.S. Patent 4,199,253. (RVSI, Hauppage, NY)

Sampson RE (1987) 3D range sensor via phase shift detection (Insert). IEEE Computer 20(8):23–24

Sasaki O, Okazaki H (1986) Sinusoidal phase modulating interferometry for surface profile measurement. And Analysis of measurement accuracy in sinusoidal phase modulating interferometry. Applied Optics 25(18): 3137–3140,3152–3158

Sato Y, Kitagawa H, Fujita H (1982) Shape measurement of curved objects using multiple-slit ray projection. IEEE Transactions Pattern Analysis Machine Intelligence PAMI-4, 6:641–649

Sato K, Inokuchi S (1985) 3D surface measurement by space encoding range imaging. Journal of Robotic Systems 2(1):27–39

Schewe H, Forstner W (1986) The program PALM for automatic line and surface measurement using image matching techniques. Proceedings Symposium International Society for Photogrammetry and Remote Sensing, Vol. 26, Part 3/2:608–622

Schlag JF, Sanderson AC, Neumann CP, Wimberly FC (1983) Implementation of automatic focusing algorithms for a computer vision system with camera control. CMU-RI-TR-83-14

Schmitt F, Maitre H, Clainchard A, Lopez-Krahm J (1985) Acquisition and representation of real object surface data. SPIE Proceedings Biostereometrics Conf., Vol. 602

Schmitt F, Barsky B, Du W (1986) An adaptive subdivision method for surface-fitting from sampled data. Computer Graphics 20(4):179–188

Schuman W, Dubas M (1979) Holographic Interferometry. Springer-Verlag, Berlin

Schwartz J (1983) Structured light sensors for 3D robot vision. Robotics Research Report No. 8, Courant Institute of Mathematical Sciences, New York University, New York

Sciammarella CA (1982) The moire method—A review. Exp. Mech. 22:418–433

SELCOM (1987) Optocator product information. Valdese, NC, US; Partille, Sweden; Krefeld, West Germany

Servo-Robot (1987) Product information. Boucherville, Quebec, Canada

Shirai Y, Suwa (1972) Recognition of polyhedra with a range finder, Pattern Recognition 4:243–250

Silvaggi C, Luk F, North W (1986) Position/dimension by structured light. Experimental Techniques: 22–25

Skolnick MI (1962) Introduction to Radar Systems. McGraw-Hill, New York

Slevogt H (1974) Technische Optik. Walter de Gruyter, Berlin, pp 55–57

Smith RC, Cheeseman P (1987) On the representation and estimation of spatial uncertainty. International Journal of Robotics Res. 5(4):56–68

Solid Photography, Inc. (1977) (now Robotic Vision Systems, Inc. (RVSI), Hauppage, NY)

Srinivasan V, Liu HC, Halioua M (1985) Automated phase measuring profilometry: A phase-mapping approach. Applied Optics 24(2):185–188

Stockman G, Hu G (1986) Sensing 3D surface patches using a projected grid. Proceedings Computer Vision Pattern Recognition Conference: 602–607

Strand T (1983) Optical three-dimensional sensing. Optical Engineering 24(1):33–40

Svetkoff DJ (Oct. 1986) Towards a high resolution, video rate, 3D sensor for machine vision. Proceedings SPIE Conference on Optics, Illumination, and Image Sensing for Machine Vision, 728:216–226

Svetkoff DJ, Leonard PF, Sampson RE, Jain RC (1984) Techniques for real-time feature extraction using range information. Proceedings SPIE—Intelligent Robotics and Computer Vision 521:302–309

Talbot H (1836) Facts relating to optical science No. IV. Phil. Mag. 9:401–407

Technical Arts Corp (1987) Product Literature. Redmond, WA

Teich MC (1968) Infrared heterodyne detection. Proceedings IEEE 56(1):37–46

Tenenbaum J (1970) Accommodation in computer vision. Ph.D. dissertation, Stanford University, Stanford, CA

Terras R (1986) Detection of phase in modulated optical signals subject to ideal Rayleigh fading. Journal of Optical Society of America A 3(11):1816–1825

Thalmann R, Dandliker R (1985) Holographic contouring using electronic phase measurement. Optical Engineering 24(6):930–935

Theocaris PS (1969) Moire fringes in strain analysis. Pergamon Press, New York

Tozer BA, Glanville R, Gordon AL, Little MJ, Webster JM, Wright DG (1985) Holography applied to inspection and measurement in an industrial environment. Optical Engineering 24(5):746–753

Tsai R (1986) An efficient and accurate camera calibration technique for 3D machine vision. Proceedings Computer Vision Pattern Recognition Conference IEEE-CS:364–374

Vest CM (1979) Holographic interferometry. Wiley, New York

Vuylsteke P, Oosterlinck A (1986) 3D perception with a single binary coded illumination pattern. Proceedings SPIE Conference on Optics, Illumination, and Image Sensing for Machine Vision, 728:195–202

Wagner JW (1986) Heterodyne holographic interferome-

try for high-resolution 3D sensing. Proceedings SPIE Conference on Optics, Illumination, and Image Sensing for Machine Vision, 728:173–182

Wagner JF (June 1987) Sensors for dimensional measurement. Proceedings Vision'87 Conference, pp 13-1–13-18

Wang JY (1984) Detection efficiency of coherent optical radar. Applied Optics 23(19):3421–3427

Wang JY, Bartholomew BJ, Streiff ML, Starr EF (1984) Imaging CO_2 radar field tests. Applied Optics 23(15):2565–2571

Wang JY (1986) Lidar signal fluctuations caused by beam translation and scan. Applied Optics 25(17):2878–2885

Wang YE, Mitiche A, Aggarwal JK (1985) Inferring local surface orientation with the aid of grid coding. IEEE Workshop on Computer Vision: Representation and Control: pp 96–104

Wei D, Gini M (1983) The use of taper light beam for object recognition. In: Robot Vision, R. Pugh (Ed.), IFS Publications, Springer-Verlag, Berlin

Will PM, Pennington KS (1972) Grid coding: a novel technique for image processing. Proceedings IEEE 60(6):669–680

Winthrop JT, Worthington CR (1965) Theory of fresnel images I. Plane periodic objects in monochromatic light. Journal of the Optical Society of America 55(4):373–381

Wuerker RF, Hill DA (1985) Holographic microscopy. Optical Engineering 24(3):480–484

Yamamoto H, Sato K, Inokuchi S (1986) Range imaging system based on binary image accumulation. Proceedings International Conference on Pattern Recognition IEEE:233–235

Yatagai T, Idesawa M, Yamaashi Y, Suzuki M (1982) Interactive fringe analysis system: Applications to moire contourogram and interferogram. Optical Engineering 21(5):901

Yeung KK, Lawrence PD (1986) A low-cost 3D vision system using space-encoded spot projections. Proceedings SPIE Conference on Optics, Illumination, and Image Sensing for Machine Vision, 728:160–172

Zuk DM, Dell'Eva ML (1983) Three-dimensional vision system for the adaptive suspension vehicle. Final Report No. 170400-3-F, ERIM, DARPA 4468, Defense Supply Service-Washington

Note added in proofs: Several uncited references have been included to provide a more complete bibliography.

Appendix: Eye Safety

Lasers are used in all types of active optical range imaging sensors. When people are exposed to laser radiation, eye safety is critical. An understanding of eye safety issues is important to the range imaging applications engineer.

Concerning the *sale of laser products* across state lines in the United States, vendors of end-user equipment containing lasers must comply with the requirements of the Food and Drug Administration's Center for Devices and Radiological Health (CDRH). Concerning the *use of laser products,* most organizations follow the ANSI Z136.1 Standard regulations. The ANSI and CDRH regulations are essentially the same except for some fine points. A simplified version of the regulations is given below. The applications engineer should consult the CDRH (1985) regulations or the ANSI (1986) regulations for complete details.

Lasers emit electromagnetic radiation that is either visible (light) or invisible (infrared or ultraviolet). When laser radiation is received by the human eye, damage may occur in the retina or the cornea depending upon the wavelength if the radiation levels exceed the maximum permissible exposure. Visible light regulations are different from invisible regulations because of the aversion response. People will blink or look away in less than 0.25 s when exposed to intense visible radiation. With invisible radiation, no such aversion response occurs although broad spectrum near-infrared laser diodes are visible to many people. Although not listed separately in official documents, the regulations may be viewed as two distinct sets of safety classes, one set for visible and another set for invisible. Within each class, two requirements must be met: (1) the average power through a standard aperture (usually 7-mm dia) must be less than the maximum average power for that class laser at every point in the field of view of the laser, and (2) the energy in any pulse received by the standard aperture must be less than the maximum energy level for that class. One subtlety important to range-imaging sensors is that the pulse repetition frequency (PRF) factor is included in ANSI regulations, but not in CDRH regulations.

For visible light (400–700 nm wavelengths), there are really five classes of lasers. Actual ratings are wavelength dependent, but the following list gives a reasonable indication of allowable average powers through the standard 7 mm diameter aperture with a 5 diopter lens.

- Class I (No Risk, Eye Safe)
  Average Power $< 0.4\ \mu W$.
- Class II (Low Power, Caution)
  $0.4\ \mu W <$ Average Power < 1 mW
- Class IIIa (Medium Low Power, Caution)
  $1 mW <$ Average Power $< 5 mW$
- Class IIIb (Medium Power, Danger)
  5 mW $<$ Average Power < 500 mW
- Class IV (High Power, Danger)
  Average Power > 500 mW

Pulse requirements are more complicated and must be computed from equations and tables listed in CDRH and ANSI regulations based on wavelength.

For invisible lasers (UV:200–400 nm, IR:700 nm–1 mm wavelengths), there are three classes:

- Class I (No Risk, Eye Safe)
  Wavelength-Dependent Regulations
- Class IIIb (Medium Power, Danger)
  Average Power $<$ 500 mW, Not Class I
- Class IV (High Power, Danger)
  Average Power $>$ 500 mW

Again, pulse requirements must be computed from equations and tables listed in CDRH and ANSI regulations based on wavelength. There are no low or medium low power categories here. However, ANSI regulations vary slightly from CDRH regulations in that they allow a Class IIIa (Caution) for infrared lasers with powers that exceed the Class I limit by less than a factor of five (Sec. 3.3.3.2, ANZI Z136.1, 1986).